Chemical Engineering Journal 475 (2023) 146041

Contents lists available at ScienceDirect

Chemical Engineering Journal

journal homepage: www.elsevier.com/locate/cej

Inorganic Nanoparticles–Driven Self–Assembly of natural small molecules in water for constructing multifunctional nanocapsules against plant diseases

Li-Wei Liu [a], Zheng-Hao Ding [a], Gang-Gang Ren [a], Guang-Di Wang [a], Xin Pan [a], Guo-Hai Wei [a], Xiang Zhou [a], Zhi-Bing Wu [a], Zhi-Chao Jin [a], Yonggui Robin Chi [a,b,*], Song Yang [a,*]

[a] National Key Laboratory of Green Pesticide, Key Laboratory of Green Pesticide and Agricultural Bioengineering, Ministry of Education, Center for R&D of Fine Chemicals of Guizhou University, Guiyang 550025, China
[b] Division of Chemistry & Biological Chemistry, School of Physical & Mathematical Sciences, Nanyang Technological University, Singapore

ARTICLE INFO

Keywords:
Inorganic nanoparticles
Natural small molecules
Nanocapsules
Plant disease
Self–assembly

ABSTRACT

Directly constructing nanoparticles through the self–assembly of natural small molecules in aqueous media presents many opportunities for crop protection; however, this special strategy is hindered by the lack of simple and cost–effective preparation methods to date. Herein, we report a facile strategy for constructing multifunctional natural nanocapsules for treating plant diseases based on the special coassembly of natural small organic molecules and inorganic nanoparticles. In aqueous conditions, uniform curcumin nanocapsules (ZnO@Cur) are assembled through electrostatic interactions, coordination effects and hydration effects as mediated by trace of nanoscale zinc oxide. The nanocapsules obtained can be further modified to enhance stability by introducing a polydopamine coating (ZnO@Cur@PDA). The antibacterial activity of ZnO@Cur@PDA against plant-pathogenic bacteria was better than that of curcumin, ZnO NPs, ZnO@Cur and zinc thiazole *in vitro*. The nanocapsules effectively kill plant–pathogenic bacteria via tight binding to the bacterial surface, inducing reactive oxygen species accumulation and disrupting bacterial cell walls. ZnO@Cur@PDA display strong activities against rice bacterial blight with protective activity of 64.0 % and curative activity of 62.2%, which is much better than commercial drugs bismerthiazol (protective activity of 33.0 % and curative activity of 38.4%) and zinc thiazole (protective activity of 38.6 % and curative activity of 31.8%). ZnO@Cur@PDA display adequate washing resistance, and low rice plant toxicity; furthermore, they are degradable. Additionally, both the inner cavities and outer surfaces of nanocapsules bear abundant sites and spaces that can be further tuned for loading other pesticide molecules or flexible construct complex multifunctional nanoparticles. Our study should encourage further development in the coassembly of organic and inorganic materials via green processes for effective and tunable nanopesticides.

1. Introduction

Nanomaterials with applications in sustainable agriculture and global food security continue to receive considerable attention [1–6]. Nanopesticides usually have higher overall efficacy against target organisms and lower toxicity toward nontarget organisms than conventional pesticides [1,7]. However, large amounts of organic solvents, surfactants and other additives are still required to prepare nanoscale pesticides by top–down methods, such as wet milling, emulsification and high–pressure homogenization [8–13]. Despite reports on numerous bottom–up methods for creating new nanomaterials, most of these methods are designed without sufficient considerations of the specific properties needed for pesticide applications [14–16]. Some methods for constructing nanopesticides involving complex processes and costly (or toxic) materials are far from ideal for obvious reasons, such as high costs and negative environmental consequences [17]. Therefore, new strategies that allow facile and green access to multifunctional nanoparticles from inexpensive and nontoxic materials are of immediate significance.

* Corresponding authors at: National Key Laboratory of Green Pesticide, Key Laboratory of Green Pesticide and Agricultural Bioengineering, Ministry of Education, Center for R&D of Fine Chemicals of Guizhou University, Guiyang, 550025, China.
E-mail addresses: robinchi@ntu.edu.sg (Y. Robin Chi), syang@gzu.edu.cn, jhzx.msm@gmail.com (S. Yang).

https://doi.org/10.1016/j.cej.2023.146041
Received 19 May 2023; Received in revised form 20 August 2023; Accepted 11 September 2023
Available online 12 September 2023

Natural small molecules and their derivatives have long been used as pesticides to help reduce crop yield losses caused by pests, pathogens, and weeds [18–35]. Natural small molecules often have particular chemical structure to achieve excellent biological activity *in vitro*. However, sometimes this can be a double–edged sword; for example, poor solubility and unsatisfying stability of some natural products lead to poor efficacy *in vivo*. Interestingly, this contradiction can be transformed into synergistic effects through morphological transformations. For example, the directed self–assembly of herbal small molecules into sustained release hydrogels is achieved to achieve long–lasting effects and minor cytotoxicity in the treatment of neural inflammation or tumors [36,37]. Baicalin (BA) and sanguinarine (SAN) can directly self–assemble through non–covalent bonds such as electrostatic attraction, π–π stacking, and hydrogen bonding to form a carrier–free binary small molecule BA–SAN hydrogel, which exhibits a synergistic inhibitory effect on Methicillin–resistant Staphylococcus aureus [38]. Berberine hydrochloride (BBR) and curcumin (CM) can be assembled into submicron particles by noncovalent interactions through solvent exchange method, and the submicron particles exhibit synergistic antimicrobial activity [39]. Controlled self-assembly of natural small molecules can produce supramolecular architectures with distinct structural features to acquire significant performance. Although there are fewer cases of crop protection, self–assembling natural nanoparticles formed by natural small molecules without structural modification is a suitable method for constructing nanopesticides due to their wide availability, multi–responsiveness, easy degradability, simple processing, and relatively low production costs [40].

However, directly constructing nanopesticides through the self–assembly of natural small molecules in aqueous media is hindered by the lack of sufficient knowledge about the ability of natural small molecules to self–assemble to form multifunctional materials. One of the challenges is that unmodified natural small molecules are difficult to assemble directly into uniform, stable nanomaterials in water without adding enormous amounts of organic solvents, surfactants, and coassembled molecules. Another challenge is to endow natural nanoparticles multifunction in crop protection, such as high adhesion to plant leaves, adequate washing resistance, permeability, and degradability. Obtaining such nanoparticles usually requires complex preparation methods. For example, curcumin is a small–molecule natural product with a wide range of antineoplastic, antimicrobial, and antioxidant activities that can be obtained in large quantities at low prices from edible plants of *Curcuma longa* species. Unfortunately, the direct application of curcumin was hindered due to its low water solubility, instability at neutral and alkaline pH, low bioavailability, and rapid elimination. Curcumin is rarely used to control plant diseases due to its unsatisfactory physical and chemical properties. Research demonstrated that the water solubility and antimicrobial activity of nanoscale curcumin markedly improved [41]. Converting unmodified curcumin into well–ordered nanostructures is challenging because curcumin easily aggregates in pure water. Conventional methods for obtaining curcumin nanoparticles typically involve using large amounts of organic solvents, surfactants, and other additives that induce the desired supramolecular interactions [39,42–44]. Methods have been developed to assemble curcumin into hybrid organic – inorganic nanoparticles using metal ions from metal salt precursors, amino acids, and cosolvents [45]. Comprehensive studies by Stenzel and coworkers have shown that curcumin assembles into capsules of 100–150 nm in size in the presence of a significant excess of fructose [46]. These studies provide insightful guidance for assembling curcumin into nanopesticides. However, surfactants and organic molecules involved in these protocols through coassembly pose obstacles to their practical applications in agriculture.

In this paper, a unique organic–inorganic hybrid method is proposed, which allows the facile and bulky preparation of multifunctional curcumin nanocapsules in water at room temperature. Organic/inorganic hybrid materials exhibit excellent functional properties for catalysis, energy storage devices, and biomedical purposes in terms of composition, structure, and morphology [47–49]. Synthetic methods for organic/inorganic hybrid materials include surface modification, self–assembly, metal–organic frameworks (MOFs), physical blending, and *in situ* deposition [47]. Typically, the surfaces of inorganic nanoparticles can be modified by physical (adsorption) and chemical (grafting) methods. However, these methods often involve organic solvents or heating and are inefficient in drug loading for small organic molecules. In addition, we need to consider the harmful effects of excessive metal exposure on non–target organisms. As a suitable model, natural nanocapsules containing trace metals are more flexible than nanospheres in constructing multifunctional nanoparticles. Specifically, this advantage is to use the less raw material to construct more nanoparticles with drug–loading cavities and modified nanoshells. In this study, we found that trace amounts of metal-based inorganic nanoparticles in water can alter the colloidal stability of curcumin and prompt curcumin to assemble into nanomaterials with different morphologies (Scheme 1a). In addition, metal-based nanomaterials have been one of the most widely studied nanopesticides, including Ag-based NMs, Ti-based NMs, Cu-based NMs, and Zn-based NMs [1]. However, excessive environmental exposure of these metal-based nanoparticles can cause side effects such as phytotoxicity and non-target toxicity [50–52]. Interestingly, trace amounts of nanometer zinc oxide (ZnO NPs) can regulate the assembly of curcumin, forming stable hybrid organic/inorganic nanocapsules in aqueous media with multiple functions. Although extremely simple to prepare, the particular heterogeneous assembly process is complex, involving the balance of electrostatic interactions, coordination effects, and hydration effects of nanoparticles, which ultimately homogenizing the curcumin system (Scheme 1b). Furthermore, our facile method without adding additives such as surfactants or other organic molecules has good ductility. The obtained nanocapsules can be further modified to enhance the photostability and thermal stability, antibacterial effect by introducing a polydopamine coating, and can be directly used as effective agents for controlling plant diseases. In addition, the nanocapsules reduce the direct exposure of ZnO NPs in the environment to reducing environmental toxicity. The natural nanomaterials with well-defined shapes and special compositions have relatively excellent performance, including effective killing of plant–pathogenic bacteria both *in vitro* and *in vivo*, sufficient washing tolerance, and low rice plant toxicity, making them practically useful in crop protection (Scheme 1c,d). Additionally, both the inner cavities and outer surfaces of nanocapsules bear abundant sites and spaces that can be further tuned to load other pesticide molecules or flexibly construct complex multifunctional nanoparticles, making the nanocapsules widely used in controlling plant diseases or human diseases. This generalizable approach provides a novel platform for the design of nanopesticides.

2. Materials and methods

2.1. Materials

ZnO NPs (99.8%, 50 ± 10 nm), ZnO NPs (99.8%, 90 ± 10 nm), TiO_2 NPs (99.8%, 40 nm), CuO NPs (99.5%, 40 nm), nano–silver (1 mg/mL, 30–50 nm), tannic acid(ACS), chitosan oligosaccharides(Molecular weight ≤ 2000) and dopamine hydrochloride (98%) were procured from Aladdin Reagents Co., Ltd. (Shanghai, China). Glutathione (reduced, 98%) and curcumin (98%) were purchased from Saen Chemical Technology Co., Ltd. (Shanghai, China), and 5,5–dithio–*bis*–(2–nitrobenzoic acid) (DTNB, Ellman's reagent, 97.59%) was purchased from Shanghai Bide Pharmatech Co., Ltd. (Shanghai, China). Carboxymethyl chitosan (Degree of substitution ≥ 80%) was purchased from Shanghai Macklin Biochemical Technology Co., Ltd. Lead citrate (3%), uranyl acetate (1%), and osmic acid solution (1%) were procured from Beijing Zhongjingkeyi Technology Co., Ltd. (Beijing, China). Eponate 12™ resin, dodecenylsuccinic anhydride [3–(2–Dodecylen–1–yl)–dihydro–2,5–furandione], *N*–methylaniline (NMA), and 2,4,6–*tris*

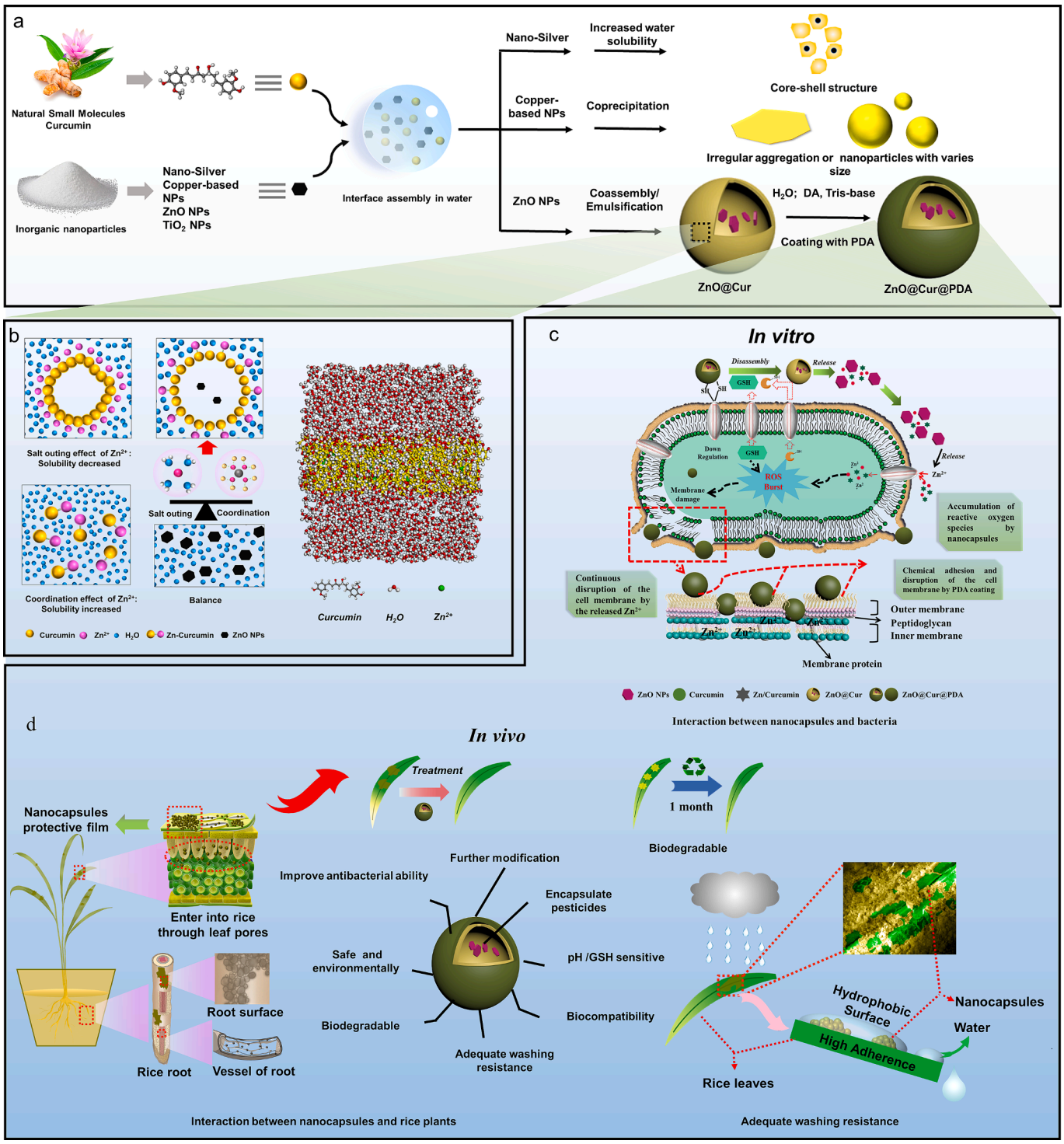

Scheme 1. Assembly of curcumin in water mediated by inorganic nanoparticles (a). ZnO NPs mediated the assembly of curcumin nanocapsules by tradeoffs with the salting–out effect and coordination effect of Zn^{2+} on curcumin assembly in water (b). Possible antibacterial mechanism of curcumin nanocapsules *in vitro*(c) and *in vivo*(d).

(dimethylaminomethyl)phenol (NMP–30) were obtained from Ted Pella, Inc. (Kanata, Canada). The hydrogen peroxide (H_2O_2) assay kit and propidium iodide (PI; 1 mg/mL) were procured from Beijing Solarbio Science & Technology Co., Ltd. (Beijing, China), and chloromethyl–2′,7′–dichlorodihydrofluorescein diacetate, acetyl ester (CM–H_2DCFDA) was purchased from Genmed Scientifics, Inc. (Shanghai, China). All the aqueous solutions were prepared using deionized (DI; 18.2 MΩ) water.

2.2. Preparation of curcumin nanocapsules

ZnO@Cur. The ZnO NPs (5.05 mg) were dispersed in double–distilled water (ddH_2O; 100 mL) via ultrasonication for 30 min (240 W, 40 KHz), and 9.9 mL of this solution was placed in a sample bottle (10 mL), to which 100 μL curcumin solution (DMSO, 20 mg/mL) was added dropwise with gentle stirring (200 rpm) to achieve a final curcumin concentration of 200 μg/mL. The experiment was repeated with various

concentrations of ZnO NPs or curcumin.

ZnO@Cur@PDA. After ZnO@Cur assembly for 5 min, 80 μL of tris base (6 mg/mL, H_2O) and 80 μL dopamine (10 mg/mL, H_2O), were added to 10 mL of ZnO@Cur colloidal solution with gentle stirring (200 rpm) in turn, then polymerized for 8 h in dark at room temperature. The colloid solution was filtered by the filter membrane(0.2 μm), then the filter cake was washed three times with ddH_2O, after freeze dring the sample was tested for characterization.

ZnO@Cur@Ta–Fe. MPN coated ZnO@Cur were prepared according to a method in the literature [53] with modification. 5 μL TA solution (20 mg/mL) and 5 μL $FeCl_3{\cdot}6H_2O$ (5 mg/mL) were successively added to the 490 μL ZnO@Cur solution at room temperature followed by brief vortexing after each addition. Then adding 500 μL 3–(N–morpholino) propanesulfonic acid buffer (20 mM, pH 7.4), and the solution was thoroughly vortexed for 5 min. The obtained particles coated by the MPN were washed three times with water to remove excess materials by centrifugation (10000 rpm, 10 min).

ZnO@Cur@Ta–Cs. 500 μL TA solution (20 mg/mL) and 500 μL Carboxymethyl chitosan (20 mg/mL) were successively added to the 10 mL ZnO@Cur solution at room temperature followed by brief vortexing after each addition. Then the solution was stirred with gentle stirring (200 rpm) for 1 h at room temperature. The obtained particles coated by the Ta–Cs were washed three times with water to remove excess materials by centrifugation (10000 rpm, 10 min).

ZnO@Cur@PDA–COS. 100 μL of chitosan oligosaccharide (20 mg/mL, H_2O) were added to 10 mL of freshly prepared ZnO@Cur@PDA colloidal solution with gentle stirring (200 rpm), then reacted for 2 h in dark at room temperature.

ZnO@Cur@PDA–Nanozymes. 100 μL of 20 mM $CuSO_4$, $Ce(NO_3)_3$, $MnSO_4$ were added to 10 mL of freshly prepared ZnO@Cur@PDA colloidal solution with gentle stirring (200 rpm) respectively, then reacted for 8 h in dark at room temperature.

Ag@Cur. 100 μL curcumin solution (DMSO, 20 mg/mL) was added dropwise to the nano–silver solution with gentle stirring (200 rpm) to achieve final nano–silver concentration of 50 μg/mL and final curcumin concentration of 200 μg/mL.

Ag–ZnO@Cur. 100 μL of nano–silver solution(1 mg/mL) and 400 μL of curcumin solution (DMSO, 20 mg/mL) were mixed, and 100 μL of the mixed solution were added to the solution containing ZnO NPs (50 μg/mL).

2.3. Characterization

High–resolution transmission electron microscopy (HRTEM; Talos F200C, FEI, USA) and field–emission scanning electron microscopy (FESEM; Nova NanoSEM^{TM} 450, FEI, USA) were used to characterize the morphologies of ZnO@Cur and ZnO@Cur@PDA. In addition, EDS (Octane Super–A, EDAX Inc., USA) was used to characterize the element distribution of ZnO@Cur and ZnO@Cur@PDA, and XPS (Thermo Scientific K–Alpha+, ThermoFisher, USA) was used to characterize the type, content, and valence of the surface elements of ZnO@Cur and ZnO@Cur@PDA. The crystalline structures of the nanoparticles were characterized using XRD (X'Pert Pro MPD, Nalytical, Netherlands); ^{1}H NMR (BioSpin–AG–400 MHz, Bruker, USA), IR (Nicolet IS50, ThermoFisher, USA), fluorescence spectrophotometry (FluoroMax®–4P, HORIBA, France), and UV–Vis spectrophotometry (UV–1900, Shimadzu, Japan) were used to analyze the variations in the molecular structure of curcumin before and after assembly. Furthermore, the hydrodynamic diameter of the nanocapsules and zeta potential of the colloidal solution were determined using multi angle particle size and high sensitive zeta potential analyzer (NanoBrookOmni, Brookhaven, USA).

2.4. Bacterial cultures and antibacterial activity

Xanthomonas oryzae pv. oryzae (Xoo) and *Pseudomonas syringae pv. actinidiae* (Psa) colonies were grown in a nutrient agar (NA) medium containing 10, 5, 1, 3, and 15 g/L of glucose, peptone, yeast extract powder, beef extract, and agar, respectively, and a bacterial monocolony was cultured in 25 mL of a nutrient broth (NB) medium containing 15, 7.5, 1.5, and 4.5 g/L of glucose, peptone, yeast extract powder, and beef extract, respectively, followed by shaking at 220 rpm for 12 h at 28 °C. The bacterial concentration was approximately 1×10^9 colony–forming units (CFU)/mL (OD_{600} 0.7–0.8), and a portion of the bacterial suspension was further diluted using the NB medium so that the final bacterial concentration was 1×10^6 CFU/mL. The bacterial suspension (50 μL; 1×10^6 CFU/mL) was mixed with varying concentrations of the NPs dispersed solution (5 mL, the concentrations of ZnO@Cur or ZnO@Cur@PDA was (ZnO 3.125 μg/mL + curcumin 12.5 μg/mL) ~ (ZnO 50 μg/mL + curcumin 200 μg/mL)) in a 15 mL glass tube to achieve a final bacterial concentration of 1×10^4 CFU/mL. For the control experiment, sterilized PBS (pH = 7.2, 1% (V/V) DMSO) or Zinc thiazole (3.125–50 μg/mL) was used instead of the nanoparticles. Thereafter, the mix solution containing bacteria were incubated at 28 °C for 8 h, and 20 μL of this solution was smeared onto NA medium plates. The number of colonies–forming units (CFU) was counted and recorded after incubation at 28 °C for 48 h. For comparison, the antibacterial activities of zinc thiazole, curcumin, and ZnO NPs at varying concentrations were tested using the aforementioned method. To further confirm the antibacterial performance of the nanocapsules against *Xoo*, the bacterial concentration in the nanocapsule dispersion (50 μL 1×10^9 CFU/mL bacterial suspension + 5 mL drug) was increased to 1×10^7 CFU/mL. Moreover, the antimicrobial activities of these drugs were tested using the double dilution method using 96 well plates. Subsequently, 100 μL NB medium was added to each well, and 100 μL drug was added to the first well for uniform mixing. This solution (100 μL) was then added to the succeeding well, and this process was repeated until the fifth well; the excess 100 μL solution was discarded. Furthermore, PBS (pH = 7.2, 0.4 mM tris–base, 1% (V/V) DMSO) was added to the sixth well as the control group, and 10 μL of bacterial suspension (1×10^9 CFU/mL) was added to each well. The 96–well plates were incubated at 28 °C for 48 h; all the steps of the experiment were performed under aseptic conditions.

(The colloidal solution of ZnO@Cur@PDA dialyzed against ddH_2O to remove dopamine hydrochloride and tris–base, then the solution was used to test the biological activity.).

2.5. Time–dependent inactivation efficiency of Xoo treated with the nanocapsules

The bacterial suspension (50 μL, 1×10^6 CFU/mL) was mixed with sterilized PBS (pH = 7.2, 0.4 mM tris–base, 1% (V/V) DMSO), ZnO NPs (50 μg/mL), curcumin (200 μg/mL), ZnO@Cur (ZnO NPs: 50 μg/mL; curcumin: 200 μg/mL), and ZnO@Cur@PDA (ZnO NPs: 50 μg/mL; curcumin 200 μg/mL) in a 15 mL glass tube to achieve a final bacterial concentration of 1×10^4 CFU/mL; the suspensions were then incubated at 28 °C for 10, 30, 90, and 180 min, respectively. Thereafter, 20 μL of this solution was smeared onto NA medium plates, and the number of CFUs was counted and recorded after incubation at 28 °C for 48 h.

$$\text{Survival Rate}(\%) = \left(C_{(A)} - C_{(B)}\right)/C_{(A)} \times 100\% \quad (1)$$

where $C_{(A)}$ and $C_{(B)}$ represent bacterial concentrations (CFU/mL) of the control and drug–treated groups, respectively.

2.6. Glutathione elimination assays

The thiol concentrations of glutathione (GSH) were quantified using Ellman's assay, wherein 300 μL GSH (2 mM, ddH_2O) and 400 μL phosphate buffer (0.1 M, pH 8.0, 1 mM EDTA) were mixed with 300 μL ZnO@Cur@PDA in an aqueous solution in a 2 mL brown centrifuge tube; this mixture was termed solution **A**. After incubating for 0–180 min at **25** °C, 10 μL of the mixture and 10 μL of DTNB (40 mg/mL, phosphate

buffer: 0.1 M, pH 8.0, 1 mM EDTA) were added to 280 μL of phosphate buffer; this solution was termed Solution **B**. Thereafter, 100 μL of solution **B** and 1.9 mL phosphate buffer were transferred into a 2 mL colorimetric dish (solution **C**), and the UV–Vis spectrum was acquired using an ultraviolet and visible spectrophotometer (UV–1900, Shimadzu, Japan) to determine the maximum absorption wavelength. Subsequently, 200 μL of solution **C** was transferred into a 96–well plate, and the absorbance was monitored at 412 nm using a microplate spectrophotometer (BioTek Synergy H1, BioTek, USA). The phosphate buffer, curcumin, ZnO NPs, and ZnO@Cur were mixed with the GSH solution as a negative control. All assays were performed in triplicate.

The concentration of GSH was calculated according to the following equation:

$$\mathrm{GSH(mM)} = ((\mathrm{A} - \mathrm{A_1})/(B - B_1)) \times 2\mathrm{mM}$$

where A represents the absorbance of the sample at 412 nm, A_1 represents the absorbance of the background sample without GSH mixed with DTNB at 412 nm, B denotes the average absorbance of the negative control at 412 nm, and B_1 represents the background absorbance of the DTNB at 412 nm.

2.7. Interaction of nanocapsules with the bacterial surface

TEM analysis. Approximately 5 mL of the bacterial suspension (1×10^9 CFU/mL) was centrifuged at 6000 rpm at 4 °C for 1.5 min. After discarding the supernatant, the bacteria were washed with 1 mL PBS thrice to remove the medium; finally, 1 mL PBS was added to resuspend the bacterial solution (5×10^9 CFU/mL). In addition, 100 μL of the bacterial solution was mixed with 5 mL of the drug solution and incubated at 28 °C for 1 h and 4 h. Thereafter, 20 μL aliquots were dropped on a carbon film coated with a copper grid (200 mesh), dried with filter paper for 1 min, and stained with uranium acetate (1%) for 10 s. The excess uranium acetate was absorbed using a filter paper, and the samples were dried at room temperature, following which they were observed and photographed via TEM (Talos F200C, FEI, USA).

SEM analysis. The bacteria were stabilized, rinsed with PBS, dehydrated in graded ethanol (30%, 50%, 70%, 90%, 100%, 100%), critical–point–dried using Leica CPD300, and gold–plated via ion sputtering (Cressington 108, Cressington, UK) successively before being observed via FESEM (Nova NanoSEM 450, FEI, USA).

2.8. Destruction of the bacterial cell membrane by the nanocapsules

The bacterial suspension was centrifuged at 6000 rpm for 1.5 min, and the supernatant was discarded. The cells were washed thrice with PBS to remove the excess medium and allowed to stand overnight in a glutaraldehyde (2.5%)–paraformaldehyde (4%) solution. The bacterial cells were washed five times with PBS to remove paraformaldehyde and glutaraldehyde and then postfixed for 1 h with osmium acid (1%). The samples were washed five times with PBS to remove osmium acid. After dehydration with an ethanol gradient (30%, 50%, 70%, 90%, 100%, and 100%), the ethanol present in the samples was replaced by an acetone solution (50% (ethanol), 100%, and 100%) and successively permeated with 33%, 66%, and 100% epoxy resin acetone solutions. The samples were transferred to an embedding mold for polymerization, and the embedded blocks were sectioned into thin slices (70–90 nm thick slices) using a Leica EM UC7 ultramicrotome. After being stained with uranium acetate (1%) and lead citrate (3%), the samples were observed and photographed via TEM.

2.9. Fluorescence microscopic analysis

The bacteria were treated with the prepared drugs for 0.5, 1.0, and 2.0 h, and the bacterial suspension was centrifuged at 6000 rpm and 4 °C for 1.5 min. Thereafter, the precipitate was washed thrice with PBS to remove the excess drug, and the bacterial cells were resuspended in 100 μL PBS, followed by the addition of the PI solution (20 μg/mL, 10 μL) or CM–H_2DCFDA (DCFH–DA, 10 μM, 2 μL), and incubated for 20 min at 37 °C in the dark. The stained bacteria were centrifuged and washed thrice with PBS and observed using fluorescence microscopy (Olympus–BX53, Olympus, Japan).

2.10. In–Vivo assay for determining antibacterial activity

The antibacterial activities of ZnO@Cur and ZnO@Cur@PDA against rice bacterial blight *in vivo* were evaluated [54]. The dispersive solutions of ZnO NPs, curcumin, ZnO@Cur, and ZnO@Cur@PDA were freshly prepared for use as test solutions. Zinc thiazole and bismerthiazol were diluted in a test solution of 50 mg/L as the positive control, and the same concentration of the solution without the compound was used as the negative control. Six–week–old rice plants (fengyouxiangzhan) were inoculated with *Xoo* using the leaf − cutting method. The curative activity was tested according to the following steps, and the test solutions were uniformly sprayed on the rice leaves after inoculating with *Xoo* for 24 h. The protective activity was similarly tested: the rice leaves were inoculated with *Xoo* after spraying the test solutions for 24 h. After 14 d of cultivation in the greenhouse, the lengths of the rice leaf lesions were measured, and the antibacterial activities of ZnO@Cur and ZnO@Cur@PDA were calculated and analyzed using the corresponding disease index. Overall, the experiment was repeated thrice.

2.11. Safety assessment of nanoparticles in rice

Rice seedlings grown for 1 month were used for the toxicity tests. Approximately 80 rice plants in each pot (30 cm × 40 cm) were exposed to ZnO NPs (50 μg/mL), curcumin (200 μg/mL), ZnO@Cur (ZnO NPs (50 μg/mL), curcumin (200 μg/mL)), and ZnO@Cur@PDA (ZnO NPs (50 μg/mL)) for five consecutive days; ddH_2O was used as the control, and three separate trials were performed for each treatment group. The average height, fresh weight, and dry weight of the above–ground parts of the plants were calculated after 1 month. Lastly, a one–way ANOVA and the least significant difference (LSD) or Games–Howell method were used to analyze all experimental data.

2.12. Distribution and conduction of ZnO@Cur@PDA on rice leaf surfaces

The rice plants at the tillering stage were sprayed with the nanocapsules solution, and rice leaves were collected a day later. The fresh leaves on the plant were rinsed thrice with ddH_2O and dried naturally. The samples of the drug spots and adjacent areas on the leaves were acquired with a hole puncher. In particular, the samples did not require any treatment and were directly observed in the low vacuum mode via SEM. A hole puncher was used to randomly sample an area of approximately 1 mm^2. The fresh leaves were adhered to the sample stage using a carbon conductive adhesive without dehydration, drying, or gold spraying. The sample surfaces were observed via SEM at low vacuum conditions with a Helix detector at 3 kV. In addition, the rice leaves were randomly cut in horizontal and vertical directions with a sharp double–edged blade, and the punctured surfaces of the rice leaves were faced upward to allow them to adhere onto the sample stage with the carbon conductive adhesive. The distribution of the nanocapsules in the rice plant was characterized using SEM under low vacuum conditions with a Helix detector at 3 kV. The distribution of the nanocapsules on or inside the rice leaves was further confirmed via EDS (Octane Super–A, EDAX Inc., USA).

2.13. Foliar distribution and washout resistance

The rice leaves were sprayed with a 30 mL ZnO@Cur@PDA solution and dried naturally. The rice leaves were then cut off and adhered to a

glass slide with double–sided adhesive tape; subsequently, images were captured using a camera with a macro lens. The sample was adjusted to an angle of 30° to the plane, and the water drop was 20 cm away from the leaf surface. Thereafter, deionized water was allowed to flow at a speed of 20 mL/min for 10 min to wash the samples. After drying, the variations in drug traces on the rice leaves were compared before and after washing. In addition, 20 μL of the ZnO@Cur@PDA solution was sequentially dropped onto the rice leaves (area of 2 cm × 6 cm) at ten distinct points to prepare six parallel samples. After natural drying, three parallel samples were used for simulating rainwater washing, and three samples were used as controls. The dried leaves were cut into pieces and added to 2 mL ethanol for ultrasonic crushing and dissolution for 10 min. The concentrations of the samples were determined using a high–performance liquid chromatography system (HPLC; 1260 Infinity II, Agilent, USA). The residual content was calculated using the following equation:

$$\text{Residual content}(\%) = (C_r/C_b) \times 100$$

where C_b and C_r denote the concentrations of the samples without washing and after washing, respectively.

2.14. Statistical analysis.

All the numerical results were calculated as mean ± standard deviation. The significance was determined using Student's two–tailed t − tests and denoted by an asterisk (*, set at $p < 0.05$; **, set at $p < 0.01$; ***, set at $p < 0.001$) unless otherwise stated. A one–way analysis of variance with LSD multiple comparison tests ($p < 0.05$) was performed to demonstrate the significant differences using SPSS 18.0.

3. Results and discussion

3.1. Interaction between curcumin and metal ions or inorganic nanoparticles in water

Structurally ordered assemblies are generally created by highly synergetic intermolecular interactions in homogeneous system [55]. Nevertheless, the assembly method for organic–inorganic hybrid nanomaterials, including homogeneous assembly processes of metal phenolic networks (MPN) and heterogeneous assembly processes such as metal organic framework (MOF) or interfacial self-assembly of metal ions and small organic molecules at the organic–aqueous interface [56]. As far as we know, metal ions can change the solubility of small molecules in water, for example, metal ions can increase the solubility of small

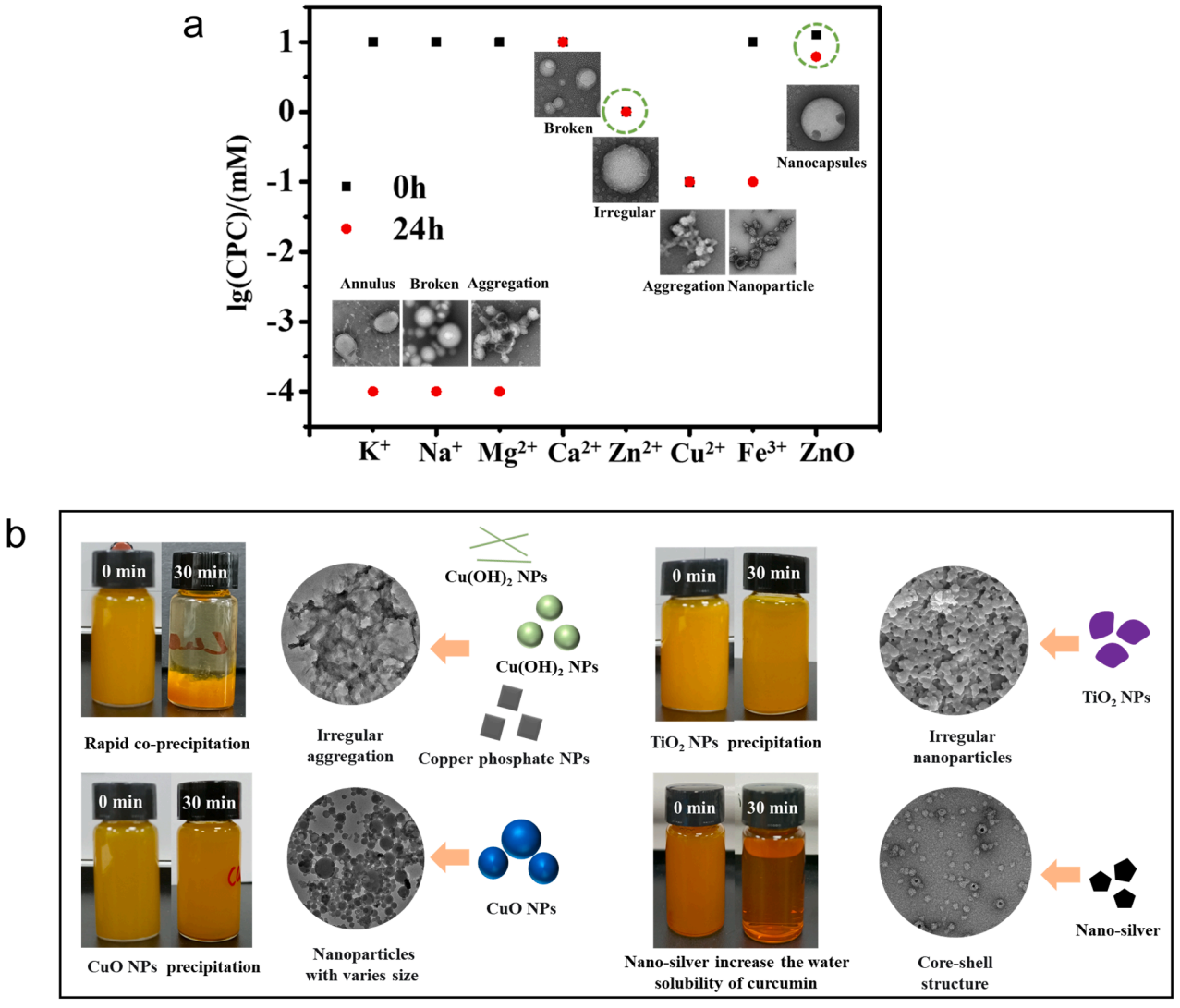

Fig. 1. The lowest precipitation concentration of different cations and the assembly morphology of curcumin (a). Inorganic nanoparticles mediated the assembly of curcumin in water–morphology diversity(b).

organic molecules through coordination effects or decrease the solubility of hydrophobic organic molecules through salting out effects. In this study, despite the anomalous results of Mg^{2+}, in general, weakly hydrated cations were not conducive to the stability of curcumin colloidal solutions, whereas the low concentration of strongly hydrated cations improved colloidal stability due to the coordination effects (Fig. 1a, S1). In addition, curcumin can be assembled into nanoparticles with different morphologies in different cationic solutions. However, the ions are often not uniformly distributed in aqueous salt solutions due to the existence of cation and anion, together with the imbalance of salting out and coordination effect, it was difficult to acquire stable and uniform nanoparticles in the above cation solutions (Fig. S1d).

Relative to metal salt precursors, metal-based nanoparticle dispersion in water provides coordination of metal ions and offers a weak hydration effect, creating multiple options for controlling the assembly of small molecules. The composition, morphology, size, and surface charge of nanoparticles affect the assembly process of curcumin in water. Briefly, the strong interaction between copper-based NPs (Cu $(OH)_2$ NPs, $Cu_4(OH)_6Cl_2$ NPs, and $Cu_3(PO_4)_2$ NPs,) and curcumin in water resulted in rapid precipitation of curcumin in 30 min (Fig. 1b, S2).

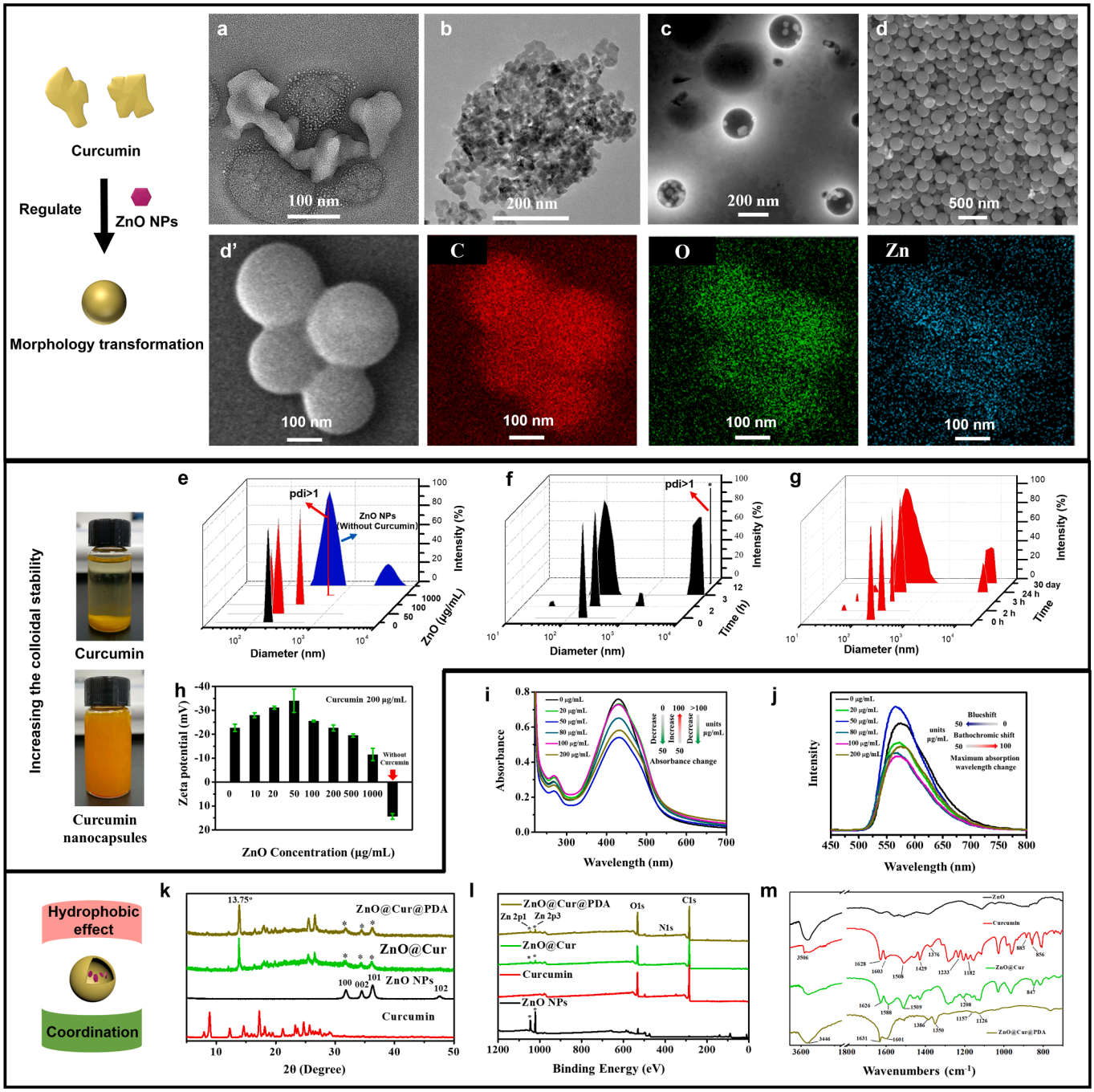

Fig. 2. Characterization of nanocapsules. TEM micrographs of curcumin (a), ZnO NPs (b), and ZnO@Cur (c) with uranyl acetate, the SEM image (d) and EDX elemental mapping results(d') of ZnO@Cur. Dynamic light scattering (DLS) particle size distribution of curcumin in various concentrations of ZnO NPs (e), particle size distribution vs. time of pure curcumin (f) and ZnO@Cur (g). Zeta potentials of nanocapsules (h) for various concentrations of ZnO NPs. UV–Vis (i) and fluorescence spectra (j) of the curcumin and ZnO NP mixture in water. XRD patterns (k) and survey XPS spectra (l) of pure curcumin, ZnO NPs, ZnO@Cur, and ZnO@Cur@PDA. FT–IR spectra (m) of the ZnO NPs, pure curcumin, and ZnO@Cur.

The precipitated material exhibited irregular nanoaggregates containing nanofilm structure with a uniform distribution of copper elements (Fig. S2e). Interestingly, silver nanoparticles as a medium can significantly improve the solubility of curcumin (Fig. 1b, S3). TEM results show that smaller curcumin particles were formed, and a large proportion of nanoparticles enclose the Ag NPs to form a core–shell structure, which may confirm the interaction between curcumin and silver nanoparticles [57]. The weak interaction between CuO NPs or TiO_2 NPs and curcumin may be due to their difficulty in releasing free metal ions in water for curcumin coordination. As a result, curcumin formed nanoparticles of varying sizes in CuO NPs solution and irregular aggregates in TiO_2 NPs solution. ZnO NPs are significantly different from other inorganic nanoparticles in the assembly of curcumin in water. Firstly, ZnO NPs have smaller particle sizes and higher water dispersibility than copper-based nanoparticles. Secondly, the initial critical precipitation concentration (CPC) value of ZnO NPs (1 mg/mL, 12.3 mM) is about 12 times that of Zn^{2+}(1.0 mM) (Fig. 1a, S4). Adding a trace amount of ZnO NPs can effectively improve the colloidal stability of curcumin. Importantly, ZnO NPs can easily mediate the formation of regular and ordered nanocapsules of curcumin in water.

Inorganic nanoparticles and small organic molecules are usually assembled at the liquid–solid interface, including physical (adsorption) and chemical (electrostatic interaction or coordination) processes. Nevertheless, curcumin cannot form a uniform coating on the surface of inorganic nanoparticles in water due to the hydrophobicity of the molecule. In previous work, the effect of inorganic nanoparticles on the assembly of hydrophobic natural small molecules in pure water was rarely discussed. Similar work focuses on the adsorption and flocculation of inorganic pollutants in natural water by porous inorganic nanomaterials. However, due to the low concentration of pollutants in natural water, the interaction of small organic molecules at the interface of inorganic nanoparticles can be considered physical–chemical adsorption [58,59]. The interesting experimental phenomenon that ZnO NPs driven curcumin to be ordered nanomaterials prompted us to study the special heterogeneous assembly process in detail.

3.2. ZnO nanoparticles mediate the assembly of curcumin nanocapsules in aqueous solution

To commence our study, a simple process involving the dropwise addition of curcumin to a stirred aqueous dispersion of ZnO NPs at room temperature was developed. Gratifyingly, curcumin nanocapsules with sizes ranging from 40 to 296 nm and a medium size of 102 nm (Fig. 2c and S6–S10) were achieved; the nanocapsules showed remarkable stability in the dark for up to 1 month, whereas the aqueous solution of curcumin precipitated after 24 h (Fig. S11). The colloidal stability of the obtained nanocapsule was further investigated by various experiments, which were highly dependent on the concentrations of the ZnO NPs and curcumin in the aqueous dispersion (Fig. S13, S14). Initially, the pure curcumin solution in water readily formed a relatively uniform nanoparticle with a particle size of 167.6 ± 2.1 nm (Fig. 2f). However, the formed particles appeared to aggregate after standing for only three hours, which occurred due to the interaction of the large number of irregular nanoparticles (Fig. 2a, S12a). Intriguingly, significantly increased colloid stability was observed by the addition of trace amounts of ZnO NPs (0.0–50.0 μg/mL) to the curcumin solution (Fig. 2e, g; S15d). The average DLS particles size and polydispersity index(PDI) of the nanoparticles correlated with the concentration of the ZnO NPs and subsequently increased with an increase in the concentration. The nanoparticles have appropriate particle size and minimum change in particle size in 24 h at 50 μg/mL. Furthermore, ζ–potential tests were conducted by detecting the positive charges of ZnO NPs in aqueous solution and the negative charge of the curcumin or ZnO@Cur colloidal solution. The zeta potential with highest absolute value, i.e., highest surface charge of the ZnO@Cur colloidal solution was obtained at a concentration of 50 μg/mL, which signified the highest stability of the colloidal solution (Fig. 2h). Ultraviolet–visible (UV–Vis) spectra illustrated that a constant maximum absorption wavelength was achieved with the addition of ZnO NPs, whereas unequivocal variations in the absorption intensity and peak shape were observed (Fig. 2i). In the visible band, the absorbance of the dispersed solution reached a minimum value at a ZnO NP concentration of 50 μg/mL (Fig. S15a). Furthermore, the fluorescence spectra indicated that the addition of ZnO NPs (0–50 μg/mL) resulted in a faint blueshift from 575 to 567 nm, which typically indicated increased hydrophobicity and reduced polarity. However, at higher concentrations ranging from 50 to 1000 μg/mL, ZnO NPs led to a bathochromic shift toward 591 nm as the concentration of ZnO NPs increased; this phenomenon implied increased hydrophilicity and hydrogen bonding accompanied by a reduction in the fluorescence intensity (Fig. 2h; Fig. S15b).

Next, we analyzed the components of the self–assembled nanoparticles produced under various conditions. X–ray diffraction (XRD) analysis revealed a new diffraction peak of the nanocapsule at 13.75° that did not pertain to curcumin or ZnO; three weak diffraction peaks pertaining to the (1 0 0), (0 0 2), and (1 0 1) planes of ZnO appeared at 31.75°, 34.44°, and 36.25°, respectively (Fig. 2k). The results showed that small amounts of unreacted ZnO NPs remained in the nanocapsules. Moreover, the nanocapsules displayed various diffraction peaks with other nanoparticles synthesized from Zn^{2+} or ZnO with curcumin, such as medi–MOF–1 [60], ZnO/curcumin nanocomposites [61], and sc–CCMOF–1 [62]. Energy-dispersive X-ray spectroscopy (EDX) mapping results revealed that the ZnO@Cur were composed of C, O, and Zn (Fig. 2d', S16). X–ray photoelectron spectroscopy (XPS) studies showed that the distributions of zinc on the surfaces of the nanocapsules were relatively low, with an atom fraction of approximately 0.66% (Fig. 2l, S17). In the XPS C1s spectra of the nanocapsules, the peaks centered at 248.8, 286.5, 287.9, 289.3, and 291.4 eV corresponded to C–C/C–H, C–O, C = O, C = C, and the π → π* satellite, respectively (Fig. S12) [63,64]. Relative to that in the XPS C1s spectrum of curcumin, the C = C content increased, the C = O content decreased, and the satellite peak of π → π* shifted toward low binding energy in the XPS C1s spectra of the nanocapsules. In the XPS O1s spectra of the ZnO NPs (Fig. S17), the binding energy at 530.3 eV was attributed to the oxygen ions (O_2^-) in the crystal lattice, the 532.1 eV peak wase ascribed to the –OH on the surface of ZnO, and the binding energy at 532.6 eV was attributed to the chemisorbed oxygen [65,66]. However, these three peaks disappeared in the nanocapsules, indicating that many ZnO NPs were not present around the nanocapsules.

The Fourier transform infrared (FT–IR) results showed that the peak at 3506 cm^{-1} was attributed to the –OH stretching of the phenol group, and the intramolecular hydrogen bonds disappeared in the nanocapsules (Fig. 2m). Certain peaks associated with the enol form varied significantly, and the intensity of the δ(COH) peaks in the nanocapsules decreased considerably (1429 and 1376 cm^{-1}); additionally, the peak at 1233 cm^{-1} (δ(COH)) disappeared in the nanocapsules. The peak at 1603 cm^{-1}, which was attributed to ν(C = O) in the nanocapsules, shifted toward 1588 cm^{-1}, thereby implying the relatively strong coordination of the carbonyl moiety [67,68]. Usually, the enol form of curcumin is more stable than the diketone forms due to the formation of stronger intramolecular hydrogen bonds. Moreover, several studies reported that the metal ions coordinating with the carbonyl and oxygen molecules on the enol group in curcumin formed more stable molecules than curcumin alone [69,70]. The hydrogen nuclear magnetic resonance (^{1}H NMR) spectrum revealed that the enol peak appeared at 16.51 ppm in curcumin; however, this peak disappeared in the nanocapsules, which could have been caused by the coordination of Zn^{2+} with curcumin (Fig. S18) [45,68]. In particular, five groups of new peaks (**ć, d́, é, f́ and ĥ**) attributed to the Zn–curcumin complex appeared in the ^{1}H NMR spectrum of ZnO@Cur, further indicating that the nanocapsules consisted of curcumin and a Zn–curcumin complex (Fig. S5, S18). Combined with transmission electron microscopy (TEM) results, we deduced that small amounts of unreacted ZnO NPs were encapsulated (Fig. S19) and that

the shells on the surfaces of the capsules could have been composed of curcumin and the Zn–curcumin complex.

3.3. Possible assembly mechanism of curcumin nanocapsules

Extremely high or low concentrations of curcumin were not conducive to the formation of nanocapsules (Fig. S14). The hydrophobicity, special symmetry, and conjugate structure of curcumin significantly contributed to nanocapsule formation. The hydrophobic nature of the phenyl rings of curcumin, along with the hydrogen bond formation ability of the side groups, is proposed to be the reason for the aggregation in water [71]. Interestingly, the assembly of nanocapsules failed under the same conditions using curcumin derivatives methylcurcumin, dimethylcurcumin, dihydrocurcumin, or tetrahydrocurcumin (Fig. 3a,

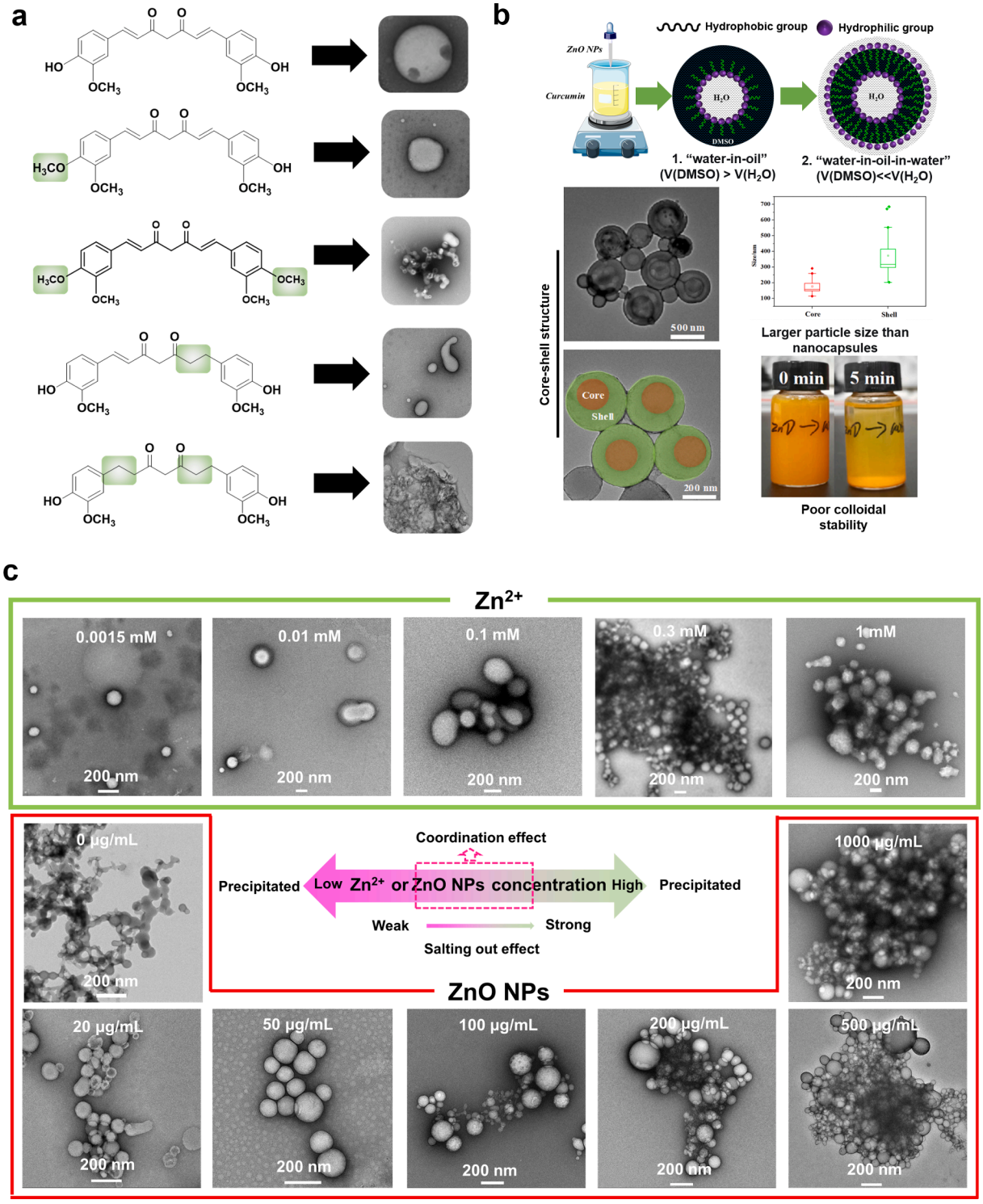

Fig. 3. (a) Morphology of curcumin derivatives assembly in water. (b) Curcumin assembly into core–shell nanoparticles with the reverse addition order of reactants. (c) Effect of Zn^{2+} or ZnO NPs concentration on the assembly behavior of curcumin in water. (d) d-1 Interfacial assembly behavior of curcumin with ZnO NPs with different morphologies and sizes; d-2: SEM(CBS) images and EDX data of ZnO@Cur nanocapsules; d-3: EDX elemental mapping results of ZnO@Cur nanocapsules contact with unreacted ZnO NPs. (e) Possible assembly mechanism of ZnO NP–mediated curcumin to construct nanocapsules in water.

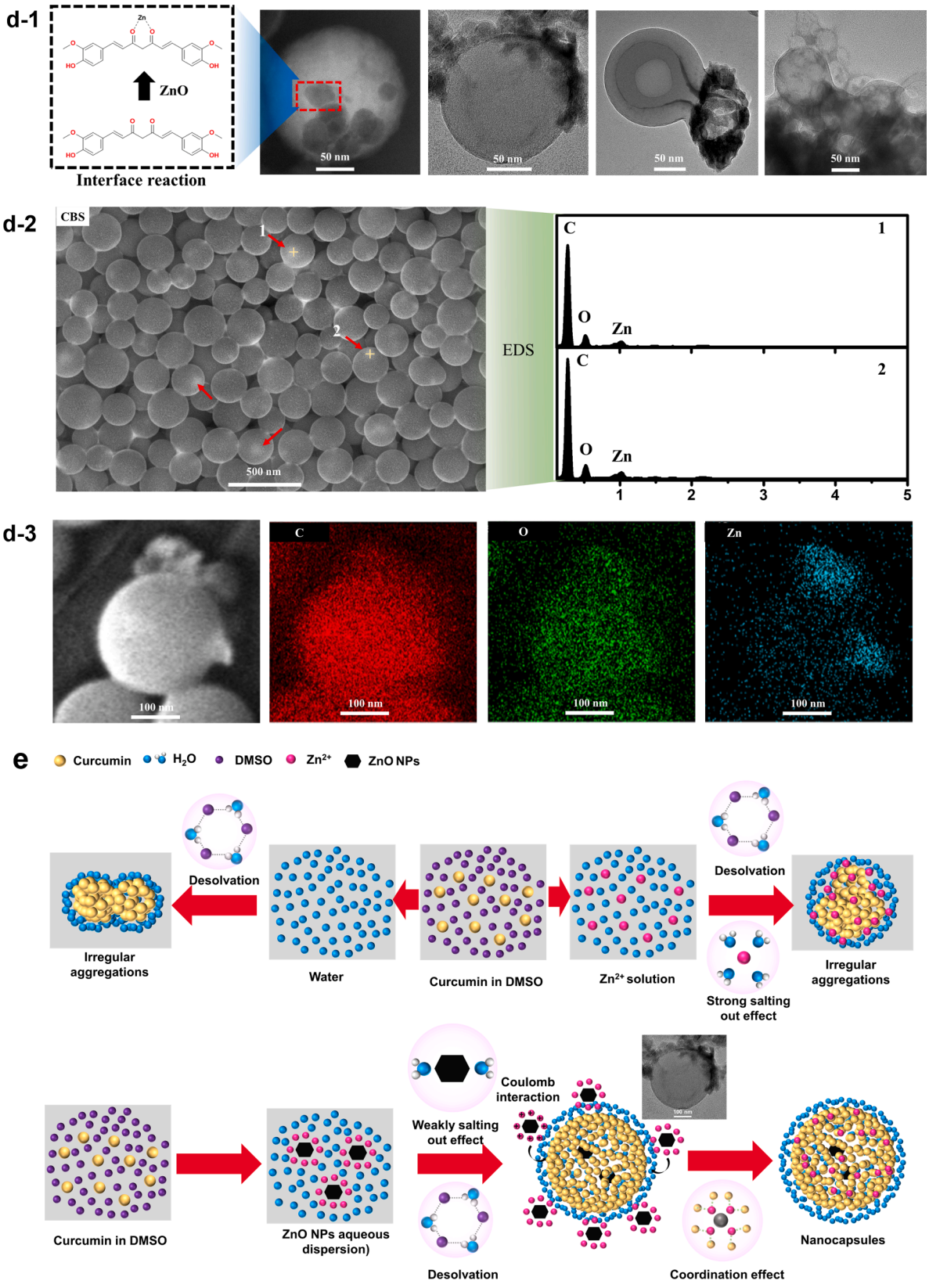

Fig. 3. (*continued*).

S20). Methylcurcumin solution has a certain colloidal stability, and the particle size is relatively uniform with the range of 60 ~ 400 nm; the nanoparticles are irregular nanoparticles, not nanocapsules. Due to the further enhancement of hydrophobicity of dimethylcurcumin, a large number of flocculent precipitates appear in its dispersible solution, and TEM showed that the precipitates are the aggregates of irregular nanoparticles. When the hydrophilic phenol hydroxyl group was successively replaced by the hydrophobic methoxy group, the polarity of the

molecule decreases and the hydrogen bond donor is reduced, and the hydrogen bond network based on the phenol hydroxyl group is destroyed, making it difficult to form regular nanoparticles. When the C = C double bond of curcumin changes to C–C successively, the hydrophobicity of the molecule is enhanced. In addition, the number of rotatable bonds increased to improve the flexibility of the molecule. As a result, dihydrocurcumin formed nanoparticles with different shapes, and tetrahydrocurcumin showed the nanofilm structure. This phenomenon could be related to changes in the molecular hydrophobicity or molecular complexation toward Zn^{2+} ions.

The desolvation of the hydrophobic surfaces of curcumin in dimethyl sulfoxide (DMSO) led to the formation of hollow aggregates because of the disruption of the hydrogen–bond networks in water. Comparatively, as a typical antisolvent regulation pattern of organic nanoparticles [72,73], after the addition of ZnO NP solution to the DMSO solution of curcumin (i.e., with the reverse added order), a wide range of nanoparticles formed in the solution as core–shell structures with larger sizes and poorer colloid stabilities (Fig. 3b). Therefore, the interactions of solute (curcumin), solvent (DMSO) and antisolvent (H_2O) were important factors in determining the assembly morphology of curcumin, and the antisolvent should always be in excess to acquire more stable nanocapsules [74]. In addition, the surface tension of the aqueous dispersion solutions did not vary significantly with different concentrations of the ZnO NPs (Table S1), which indicated that the formation of nanocapsules was independent of the surface tension of the system—a typical kinetic factor in self–assembly [45].

The assembly mode of the unique inorganic-organic hybrid nanoparticle was highly distinct from the conventional strategy driven by noncovalent forces between organic molecules or the ZnO/curcumin nanocomplexes prepared with surface functionalization, adsorption or coating. Relative to the system involving metal salt precursors, the coassembly of nanoparticles and curcumin often exhibited a gentler interaction force because of the differences (i.e., mobility, solvability, and hydration effect) between nanoparticles and metal ions. First, the dispersed phase of ZnO NPs in colloidal solution divided the aqueous solution into many tiny microenvironments. Moreover, the weaker intensity of the Brownian motion of nanoparticles in colloids than that of the thermal motion of ions dramatically influenced the diffusion of curcumin in water (Fig. S21) and effectively reduced the aggregation of assembled particles. Second, the curcumin nanoparticle system showed an interesting salting–in effect at low concentrations of ZnO NPs while displaying a salting–out effect at high concentrations (Fig. 3c). At a 50 μg/mL concentration of ZnO NPs, the TEM results demonstrated relatively regular morphologies and uniform particle sizes for the formed nanocapsules. Other solutions at lower or higher concentrations failed to form uniform and regular nanocapsules. The key concentration effect wase explained by various hydration and coordination effects between Zn^{2+} ions and curcumin at different concentrations of ZnO NPs (Fig. S4–S5), which significantly affected the self–assembly process of curcumin. At the optimal 50 μg/mL concentration, the ZnO NPs featured a relatively weak hydration effect and gradually released Zn^{2+} ions in the system (Table S2), thereby offering comprehensive means to form nanocapsules by gentle coordination with curcumin through special interfacial interaction. The interfacial interaction between ZnO NPs and curcumin shell was confirmed by point and map scanning data of EDX. TEM and SEM data showed that fully dispersed ZnO NPs with small particle sizes (~50 nm) could drive curcumin to form uniform nanocapsules. Black spots (TEM)or bright spots (SEM, backscattered electron (CBS) imaging) in nanocapsules may indicate that the nanocapsules contain ZnO or Zn-curcumin (Fig. 3d). However, curcumin was assembled into nanocapsules with different sizes or even aggregates in the solution containing ZnO with large particle sizes (Fig. S22–S23). The interfacial fusion of ZnO and curcumin indicates the feasibility of constructing organic–inorganic hybrid nanomaterials in pure water. As a result, the addition of ZnO NPs perfectly balanced the interactions among zinc, curcumin, dimethyl sulfoxide, and H_2O to provide simple and rapid access to ZnO@Cur nanocapsules with substantial stability (Fig. 3e).

The traditional construction methods for nanocapsules usually use polymers or well–designed amphiphilic block molecules as raw materials, and these methods require a large amount of organic or inorganic materials as templates or to prepare precursor molecules via complex chemical modifications [75–80]. It will be a very useful strategy to construct high–activity nanocapsules with nontoxic natural small molecules as nano intermediaries. The assembly process of natural small molecules in water is usually relatively simple, and the phenomenon is unique and fascinating [55]. However, the self–assembly of natural small molecules in water is difficult to control in artificial systems [81,82]. For instance, the self–assembly of curcumin nanospheres or nanocapsules driven by coordination effects or noncovalent interactions usually requires a certain proportion of cosolvent or other organic molecules [45,46,69,83]. Herein, inorganic nanoparticles were used as a simple medium for regulating curcumin assembly into nanocapsules in water. Obviously, this simplified process without adding surfactants or other organic molecules is beneficial to industrial production. We stress that this simplicity of preparation does not imply the simplicity of the interactions between curcumin and ZnO NPs. The particular heterogeneous assembly process could be explained by the balance of electrostatic interactions, coordination effects, and hydration effects of the nanoparticles homogenizing the curcumin system. We further confirm that the homogenization effect is closely related to the composition, morphology, and particle size of metal oxide NPs. However, compared with other precursors, a suitable concentration of ZnO NPs with appropriate particle size is more conducive to the formation of curcumin nanocapsules. Fortunately, the method is simple and has good extensibility. For example, copper–based nanoparticles were used to drive the construction of glutathione from disordered to ordered organic–inorganic hybrid nanocapsules (Fig. S24a). The formation of nanoparticles involves complex driving forces such as redox, coordination, and hydrogen–bond interaction effects on the interface of copper-based nanoparticles. Whereas, glutathione reacts with soluble Cu^{2+} to form a hydrogel in homogeneous system (Fig. S24c). The interfacial reaction of inorganic nanoparticles with organic nanoparticles was conducive to the metal ions incorporated into the nanocapsule system at room temperature to enhance the biological activity (Fig. S24b). Although the heterogeneous assembly process is unique, the method has shown broad application prospects in driving natural small molecules or synthetic molecules to construct nanoparticles in water.

3.4. Template polymerization

As a biologically interesting natural product, curcumin in the form of nanocapsules offers a unique platform for the preparation of bioactive nanoparticles or pesticide nanocarriers due to its colloidal stability, pH response characteristics and facile degradation (Fig. S25–27). However, curcumin nanocapsules are difficult to directly apply in crop protection due to their fragility and weak surface interactions with phytopathogens or plants (Fig. S28). Usually, the phenolic groups on the surfaces of nanocapsules enable further interactions with building blocks via noncovalent interactions to construct multifunctional nanoparticles. To enhance the stabilities of the nanocapsules for practical application, chitosan, polydopamine (PDA) and metal–phenolic networks are successfully coated on the surfaces of curcumin nanocapsules (Fig. 4a–c). Because curcumin is sensitive to organic solvents, strong acids and bases, it is difficult to obtain rigid coatings, such as silica and metal–organic frameworks. However, polydopamine–modified curcumin nanocapsules show improved uniformity and stability. Similar diffraction peaks for both ZnO@Cur@PDA and ZnO@Cur are observed in their XRD spectra (Fig. 2i). The distribution of trace nitrogen on the surfaces of the nanocapsules from the XPS spectra(Fig. 2l). EDS data clearly indicated the presence of the O, N, Zn (Fig. 4c5-8). The FTIR spectrum of ZnO@Cur@PDA (Fig. 2m) reveals the intensity of characteristic peaks

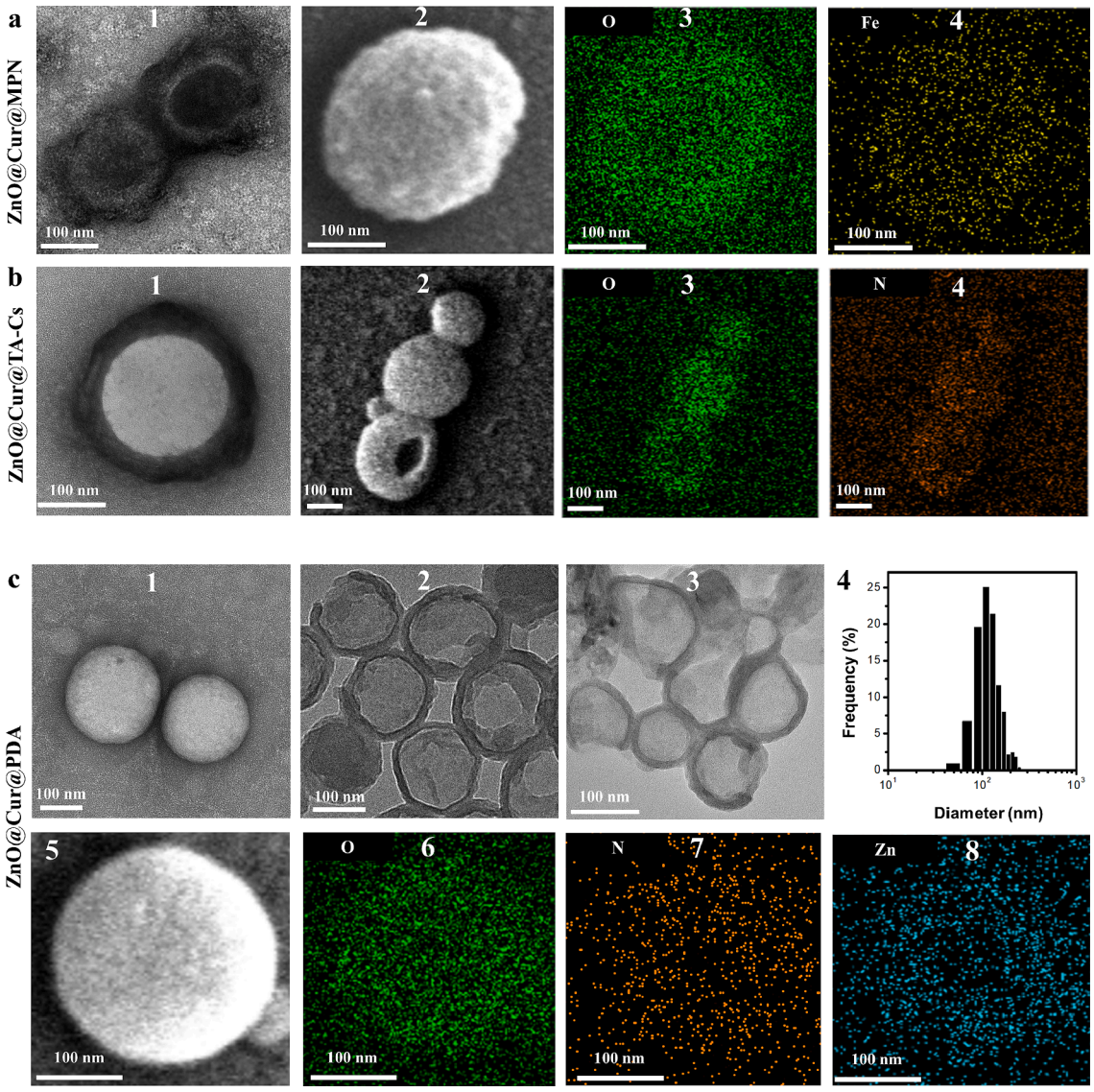

Fig. 4. (a) MPN (i.e., Fe(III)–TA)–coated ZnO@Cur particles (1: TEM image; 2:SEM image; 3–4: EDX elemental mapping data). (b)Polyphenol–carboxymethyl chitosan network–coated ZnO@Cur particles (1: TEM image; 2:SEM image; 3–4: EDX elemental mapping results). (c)Polydopamine–coated ZnO@Cur particles (1: Negative staining with 1% uranyl acetate; 2: Without negative staining; 3: Hollow structures after removal of the ZnO@Cur@PDA core; 4: Particle size distribution of ZnO@Cur@PDA; 5: SEM; 6–8: EDX elemental mapping results).

attributable to curcumin change to be weaker. The peaks between 1631 and 1601 cm^{-1} were associated with bending of N–H of the amine group in the PDA coating and stretching vibrations of C–C aromatic rings. These evidences further confirmed that curcumin was successfully encapsulated by PDA. In comparison to the ZnO@Cur particles, the PDA–coated nanoparticles (ZnO@Cur@PDA) feature greater diameters that are directly observed without negative staining (Fig. 4c-1, c-2, c-4) and a higher content of zinc on the shell (Fig. S17b). Additionally, the ZnO@Cur@PDA nanocapsules generate damaged hollow particles when the coated particles are immersed in ethanol to remove the curcumin template (Fig. 4c-3). The successfully prepared solution is a homogeneous and stable colloid with a blue–green or dark–green color (Fig. S29). Upon passing the solution through a 0.22 μm filter membrane, the filtrate is clear, transparent and free of curcumin, and numerous nanocapsules are distributed on the filter cake (Fig. S30). The loading efficiency of curcumin in ZnO@Cur@PDA nanocapsules was 64.71%±0.14%. As shown in Fig. S31, after 120 min of UV irradiation (256 nm, 100 μJ/cm2), the concentration of curcumin in the curcumin solution and ZnO@Cur solution degraded to 49.7% and 58.7% of the initial concentration, respectively. However, the concentration of curcumin in the ZnO@Cur@PDA solution was only reduced by 4.5% of the initial concentration. The colloidal stability of the curcumin solution becomes worse after heating at 60℃ for 10 min, and the colloidal solution appears flocculation. In contrast, ZnO@Cur and ZnO@Cur@PDA solutions maintained good colloidal stability after heating for 2 h. The concentration of curcumin in the curcumin solution and ZnO@Cur solution degraded to 84.4% and 90.0% of the initial concentration, respectively. The concentration of curcumin in ZnO@Cur@PDA nanocapsules was almost unchanged. The above results showed that the stability of the nanocapsules was significantly improved by coating with PDA. ZnO@Cur@PDA has a good prospect for controlling plant disease in the actual field environment.

3.5. *Antibacterial activities and mechanisms of ZnO@Cur and ZnO@Cur@PDA*

Curcumin nanocapsules are of considerable interest in crop protection because of their special compositions and ordered nanostructures.

Xanthomonas oryzae pv. oryzae (Xoo) and *Pseudomonas syringae pv. actinidiae* (Psa) are typical and important plant pathogenic bacteria. Due to the bacterial resistance and nontargeted toxicity characteristics of conventional antibacterial agents, there is still a lack of effective alternative agents to control these bacterial diseases [84–88]. Strikingly, both ZnO@Cur and ZnO@Cur@PDA display significant inhibitory activity against Xoo and Psa *in vitro,* while curcumin alone shows negligible antibacterial activity (Fig. 5a–5c; S32–S35). When the bacterial concentration was ~ 1×10^4 CFU/mL, the minimal bactericidal concentrations (MBC) of curcumin, zinc thiazole, ZnO, ZnO@Cur and ZnO@Cur@PDA for Xoo were > 200, 25.0, 6.25, 6.25, and < 3.125 μg/mL, respectively. The number of bacterial colonies obtained after treatment with the nanocapsules ($(6.67 \pm 0.76) \times 10^2$ CFU/mL) was less than that obtained after treatment with the ZnO NPs ($(2.57 \pm 0.30) \times 10^3$ CFU/mL) at a concentration of 3.125 μg/mL ($p < 0.01$, t–test; Fig. 5a (2)), which demonstrated that the sterilization effect of the nanocapsules was superior to that of the ZnO NPs. To further verify the sterilization effect of nanocapsules on *Xoo*, the bacterial concentration was increased to ~ 1×10^7 CFU/mL, the MBC of ZnO@Cur and ZnO@Cur@PDA for Xoo were 12.5 and 6.125 μg/mL, respectively (Fig. S31). A similar inactivation efficiency for Psa could be achieved using the nanocapsules, and ZnO@Cur and ZnO@Cur@PDA exhibited bactericidal activities superior to ZnO NPs and zinc thiazole at a concentration of 3.125 μg/mL(Fig. 5a(3)). The bacteriostatic activity of nanoparticles in nutrient medium were also carried out by broth dilution method on 96 microwell plate. Fig. S34 indicated that the MIC of Zinc thiazole, ZnO, ZnO@Cur, ZnO@Cur@PDA and curcumin against Xoo and Psa were both 25.0, 12.5, 6.25, 3.12 and > 100 μg/mL, respectively.

The role of curcumin in the nanocapsule system is not only as a skeleton but also as an antibacterial ingredient Although curcumin has no apparent inhibitory activity on Xoo and Psa, this may be due to the low solubility of curcumin in pure water, which is easy to form disordered aggregates in water, resulting in weak interaction between drugs and bacteria. (Fig. S53). Previous studies have suggested that increasing the solubility or decreasing the particle size of curcumin in water can improve its antibacterial activity [41,89]. Therefore, nanoscale curcumin (ZnO@Cur NPs) may play some positive role in antibacterial activity via enhancing the interaction with bacteria. ZnO NPs is an essential component of nanocapsules, including encapsulated ZnO NPs and converted into Zinc-Curcumin complex in the shell. Although ZnO NPs have a strong antibacterial effect against Xoo and Psa, it is weaker than ZnO@Cur and ZnO@Cur@PDA nanoparticles. The addition of curcumin enhanced the bactericidal effect rather than reducing that, which revealed the synergistic effect of the two substances. SEM results revealed that the ZnO NPs did not interact much with the bacterial surface(Fig. S43); additionally, TEM images confirmed the absence of ZnO NPs around the bacteria(Fig. S38), whereas ZnO@Cur@PDA was uniformly distributed around the bacteria(Fig. 5c(3)-c(4), 5d(3); S39-S42). The antibacterial mechanism of the ZnO NPs may have involved the particle size effect, surface action, and the release of reactive oxygen species (ROS) and Zn^{2+}, but the agglomeration of ZnO NPs in water or nutrient medium prominently diminished these effects. Consequently, the probability of contact with the bacteria decreased for the nanoparticles that inhibited the antibacterial effect. The number and surface area increased for the same mass of ZnO@Cur and ZnO@Cur@PDA if the nanoparticles were hollow capsules instead of nanospheres or irregular aggregates, because these stable and dispersive nanoparticles could create more opportunities to come in contact with the bacteria. This indicated that the aggregation forms of the drug molecules in water determined their biological activity. In addition, the experiment results of ROS accumulation, membrane potential change, and membrane damage confirmed that the interaction between ZnO@Cur and bacteria was stronger than that between ZnO NPs and bacteria.

The distinct biological activities of the ZnO@Cur@PDA nanocapsules might be attributed to two different pathways. First, the formed nanocapsules tend to closely bind with bacteria, probably due to the high chemical affinity between Zn^{2+} or coated PDA and the amino acid residues of the bacterial membrane (Fig. 5c; S38–S42) [90–92]. Consequently, the contact interaction helps damage the outer and inner membranes of bacteria (Fig. 5d; S44–S50, S52;). A second mechanism involves decreased glutathione over time upon treatment with ZnO@Cur@PDA nanocapsules (Fig. 5b(2)–(3)). The consumption of glutathione results in a burst of ROS in the bacteria since plant pathogenic bacteria, such as Xoo, have weak redox systems to remove exogenous ROS (Fig. 5b(1), Fig. S51), which ultimately leads to the death of the bacteria [93,94]. The strong adhesive and functionalization of the PDA coating enhances the interaction between bacteria and nanocapsules to improve the antibacterial ability. The excellent antibacterial effect of the nanocapsule is the result of the rational assembly of ZnO NPs, curcumin and polydopamine. Notably, we find a strong interaction between the nanocapsules and plant viruses, leading to the passivation effect of the nanocapsules on tobacco mosaic virus. Therefore, the strong surface interaction of nanoparticles is a key factor in the design of nanopesticides (Fig. S48). The detailed data, results analysis and discussion are given in S32–52.

3.6. Controlling effect of ZnO@Cur and ZnO@Cur@PDA on bacterial blight in rice in vivo

Notably, the PDA–coated ZnO@Cur@PDA nanocapsule features considerably improved protective and therapeutic activities against rice bacterial blight relative to ZnO@Cur and the commercial drugs bismerthiazol and zinc thiazole (Fig. 6b, S55). In particular, ZnO@Cur@PDA are affixed to the surface of the rice leaf as a protective film by the formation of many nanocapsules (Fig. 6a, S56–S61). The distributions of the nanocapsules do not show significant changes after washing with double distilled water (ddH_2O, 20 mL/min for 10 min); the residual amount of nanocapsules still reaches 68.4% (calculated based on the curcumin content), as demonstrated in Fig. 6g. The substantial washing resistance of the nanocapsules might arise from the strong interactions of the nanoparticles with the rice leaf surface and the unique adhesion and water insoluble of the PDA coating. Furthermore, nanocapsules are detected in the rice leaves after spraying ZnO@Cur@PDA for 24 h (Fig. 6a, S62–63), implying that the nanocapsules may readily enter the rice plant through the leaf pores (Fig. S61), which might be the reason for the improvement in curative activity of the PDA–coated nanocapsules. In addition, the wettability of the nanocapsules on the rice leaf surface can be effectively improved through adding trace amount of sodium dodecyl sulfate (SDS). SEM results revealed that the nanoparticles can be effectively dispersed on rice leaves, while their particle size and morphology are not significantly affected. (Fig. S65).

3.7. Safety evaluation of ZnO@Cur and ZnO@Cur@PDA in rice plants

ZnO@Cur@PDA is composed of ZnO NPs, curcumin, trace of Zn-curcumin and polydopamine. These substances have been widely used in food and biomedicine fields, and are all safe for humans and environment [95–98]. The effects of nanocapsule exposure on the growth of rice plants were studied using a potted plant experiment in a greenhouse. After spraying with a normal dose of ZnO@Cur and ZnO@Cur@PDA for 1 d, there was no significant variation in rice growth relative to that in the group treated with ddH_2O (Fig. S66). Thus, we further investigated the safety of nanocapsules for rice plants under high − dose exposure. As shown in Fig. S67, the rice leaf tips turned yellow after treatment with curcumin, ZnO@Cur, and ZnO@Cur@PDA at normal doses for five consecutive days. This phenomenon probably occurred because a large amount of the drug covered the surface of rice leaves, thereby affecting photosynthesis. However, the growth of the rice plants recovered after terminating the drug treatment, and the drug residues on the surfaces of rice leaves disappeared after 1 month (Fig. S67). After nanocapsule exposure, the biomass of rice did not vary significantly from that of the control group, and it was greater than that

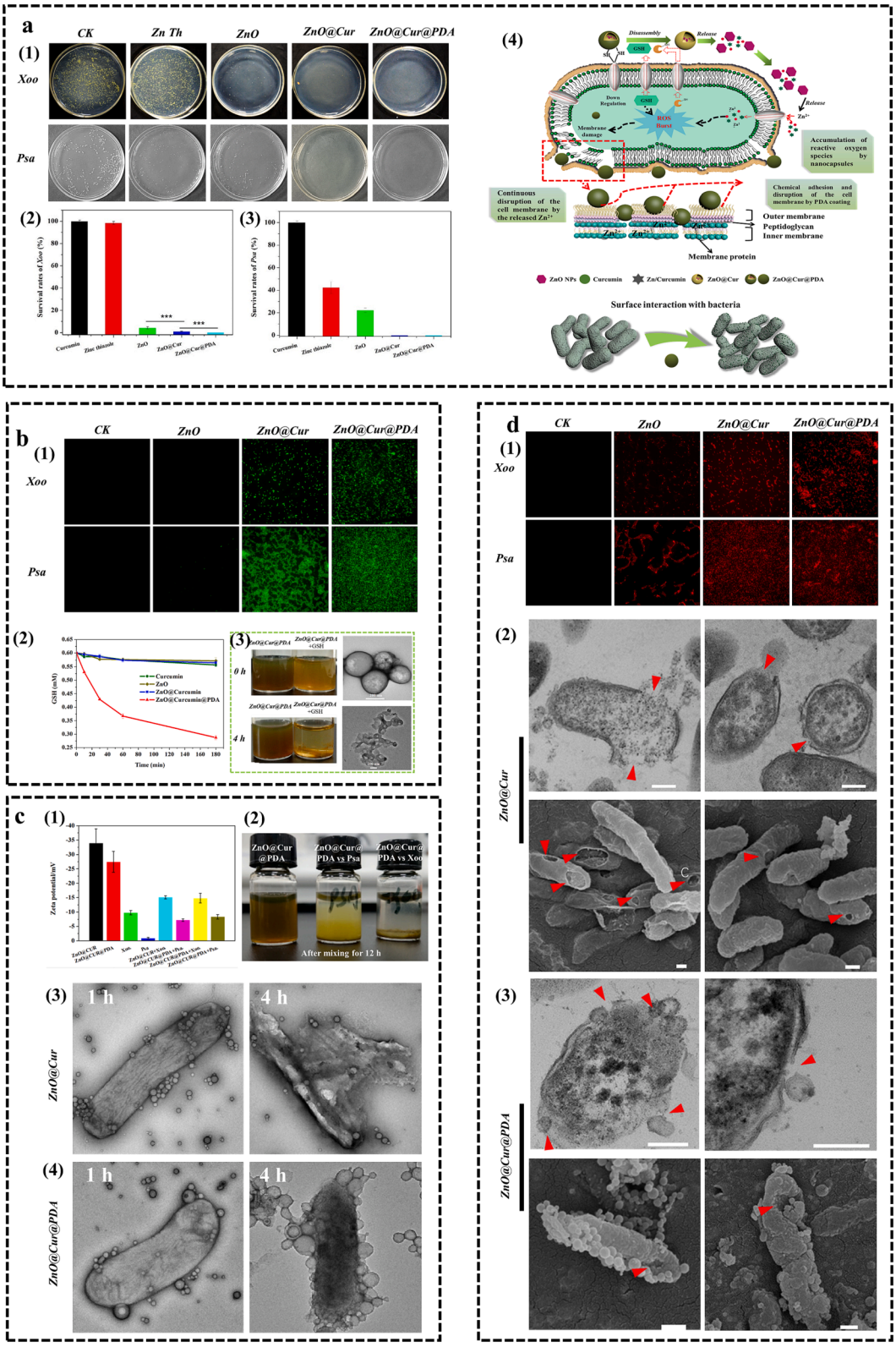

Fig. 5. Antibacterial activity of the nanocapsules (a): Agar plate photographs (1) and survival rates of Xoo (2) and Psa (3) treated with different drugs at the concentration of 3.125 μg/mL. Possible mechanisms for the potential antibacterial activities of ZnO@Cur and ZnO@Cur@PDA (4). ROS accumulation in bacteria (b): Fluorescence images of Xoo and Psa incubated with different drugs for 30 min and subsequently stained with CM–H_2DCFDA, respectively (1); Glutathione elimination curves (2); Glutathione (GSH) could change the colloidal stability and morphology of ZnO@Cur@PDA (3). The surface interaction between the nanocapsules and bacteria (c): Effects of the bacteria and nanocapsule interactions on the zeta potential (1) and the colloidal stability (2) of the mixed solution; Representative TEM images of Psa cells exposed to ZnO@Cur (3) and ZnO@Cur@PDA (4) for 1 or 4 h. Nanocapsules caused bacterial cell membrane disruption (d): Fluorescence images of Xoo and Psa incubated with drugs for 1 h and subsequently stained with propidium iodide (PI) (1); (k) Representative TEM images and SEM images of Psa cells incubated with ZnO@Cur (2) and ZnO@Cur@PDA (3) for 1 h. The red arrow indicates the disrupted cellular membrane. (For interpretation of the references to color in this figure legend, the reader is referred to the web version of this article.)

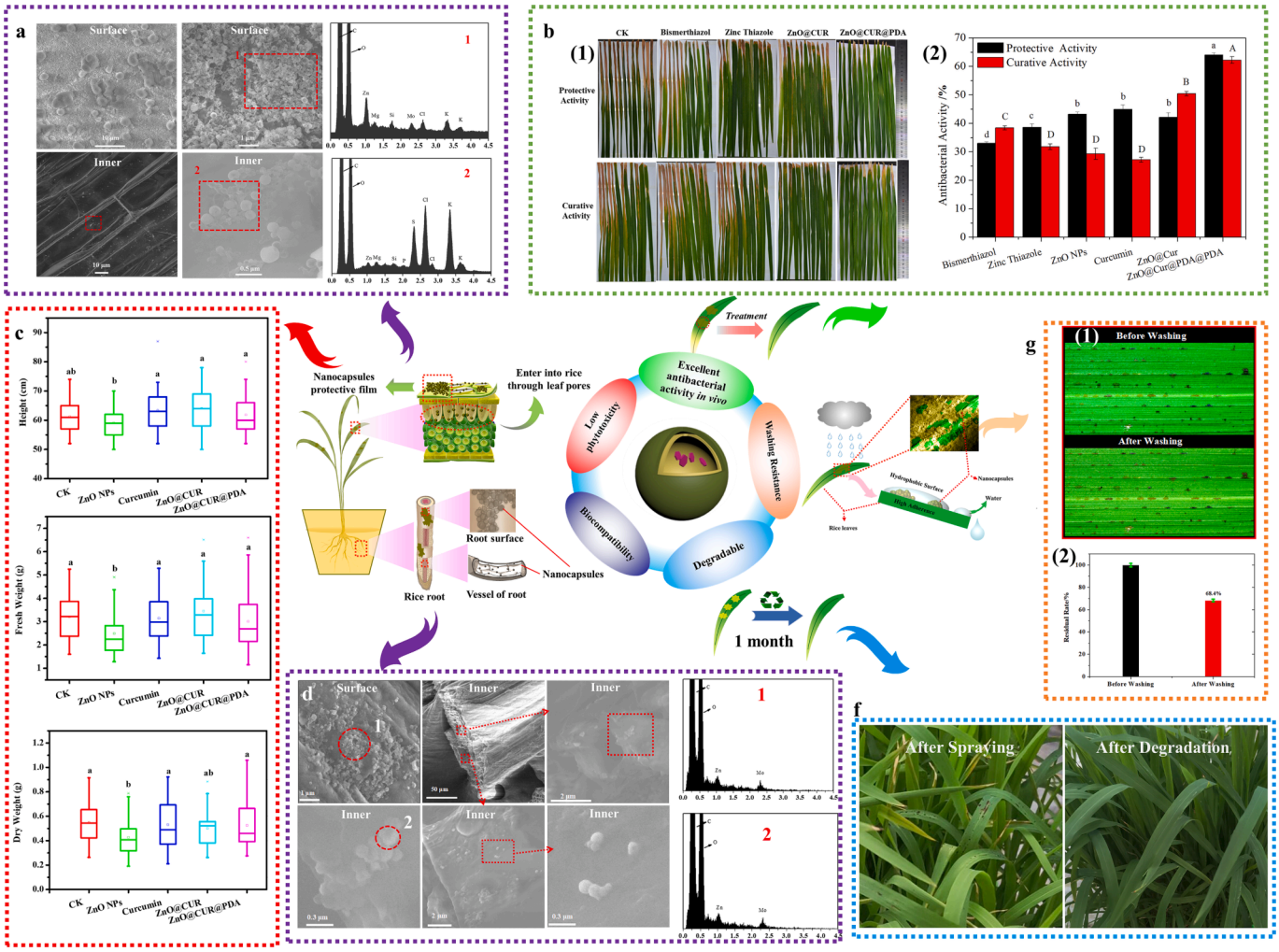

Fig. 6. Representative SEM and EDS images of ZnO@Cur@PDA distribution on the surface of and inside the rice leaves (a). Antibacterial activity of nanocapsules *in vivo* (b): Lengths of the lesions on the clip–inoculated leaves measured on day 14 for the protective and curative activities of different drugs against bacterial blight in rice (1) Histogram of the therapeutic and protective activity data (n = 3; ANOVA; Tukey HSD; $p < 0.05$) (2). After five consecutive days of exposure to different drugs, the average plant height, average fresh weight, and dry weight of the shoot parts of the plants were calculated after 1 month (n > 30) (c). ZnO@Cur@PDA could adhere to the rice root surface and could travel via the root vascular system (d). ZnO@Cur@PDA can be completely degraded within 30 days (f). Distribution and residual rate of ZnO@Cur@PDA on the rice leaves before and after washing with ddH_2O (g).

of the ZnO NP treatment group after 1 month (Fig. 6c). In addition, two–week–old rice seedlings were cultured in a ZnO@Cur@PDA solution for three consecutive days. The results indicated no inhibition of seedling growth relative to that in the control group (Fig. S68c). Furthermore, the taiphenol blue staining method was used to evaluate the toxicity of the nanoparticles on root cells; the stain did not enter the living cells, instead entering the dead cells and staining them blue. Thus, the roots treated with the nanocapsules were not dyed blue, signifying that ZnO@Cur and ZnO@Cur@PDA posed no evident toxicity to root cells within 72 h (Fig. S68c). Furthermore, the microstructure of the root tissue of rice was observed under an optical microscope. In contrast to that in the blank control group, the microstructure of the root tissue exhibited no significant variation after treatment with the nanocapsules for 72 h (Fig. S68b).Scanning electron microscopy (SEM) results revealed the attachment of numerous nanocapsules to the root surface that entered the root interior (Fig. 6d). Toxicological tests of ZnO@Cur and ZnO@Cur@PDA on rice plant and root cells showed their excellent biocompatibility and biodegradability properties (Fig. 6f). In the actual field application, ZnO@Cur@PDA nanocapsules will inevitably be irradiated by ultraviolet light or exposure to reactive oxygen species (ROS) and glutathione in plants, which leads to the nanocapsules degrading slowly rather than accumulating in plants [99–102]. On the other hand, the main components of nanocapsules have been confirmed that there are no significant side effects even if ingested directly into the body. Moreover, the main components of nanocapsules and their degradation products are very low in the plant, which has almost no side effects on biosafety.

3.8. Functional expansion of curcumin nanocapsules

The prospect of nanocapsules constructed by small–molecule natural products prompted us to construct multifunctional active nanoparticles for versatile applications (Fig. 7a). By using ZnO@Cur@PDA as a template, we preliminarily established a hollow capsule–nanocase system ZnO@Cur@PDA/nanozymes and a chitosan oligosaccharide–encapsulated nanocapsule delivery system ZnO@Cur@PDA–COS (Fig. 7c–d; S70–73). Notably, our protocol involved fewer raw materials and shorter synthetic steps compared with the preparation of nanozyme–loaded nanocapsule systems that use silica or polymers as templates [103]. Attempts to construct particular inorganic-organic hybrid nanoparticles by assembling natural small molecules, such as silver–loaded curcumin nanocapsules, also gave inspiring results (Fig. 7b; S74). In addition, a novel nanoparticle ZnO@Cur-Beb was constructed by the co-assembly of curcumin and berberine hydrochloride mediated

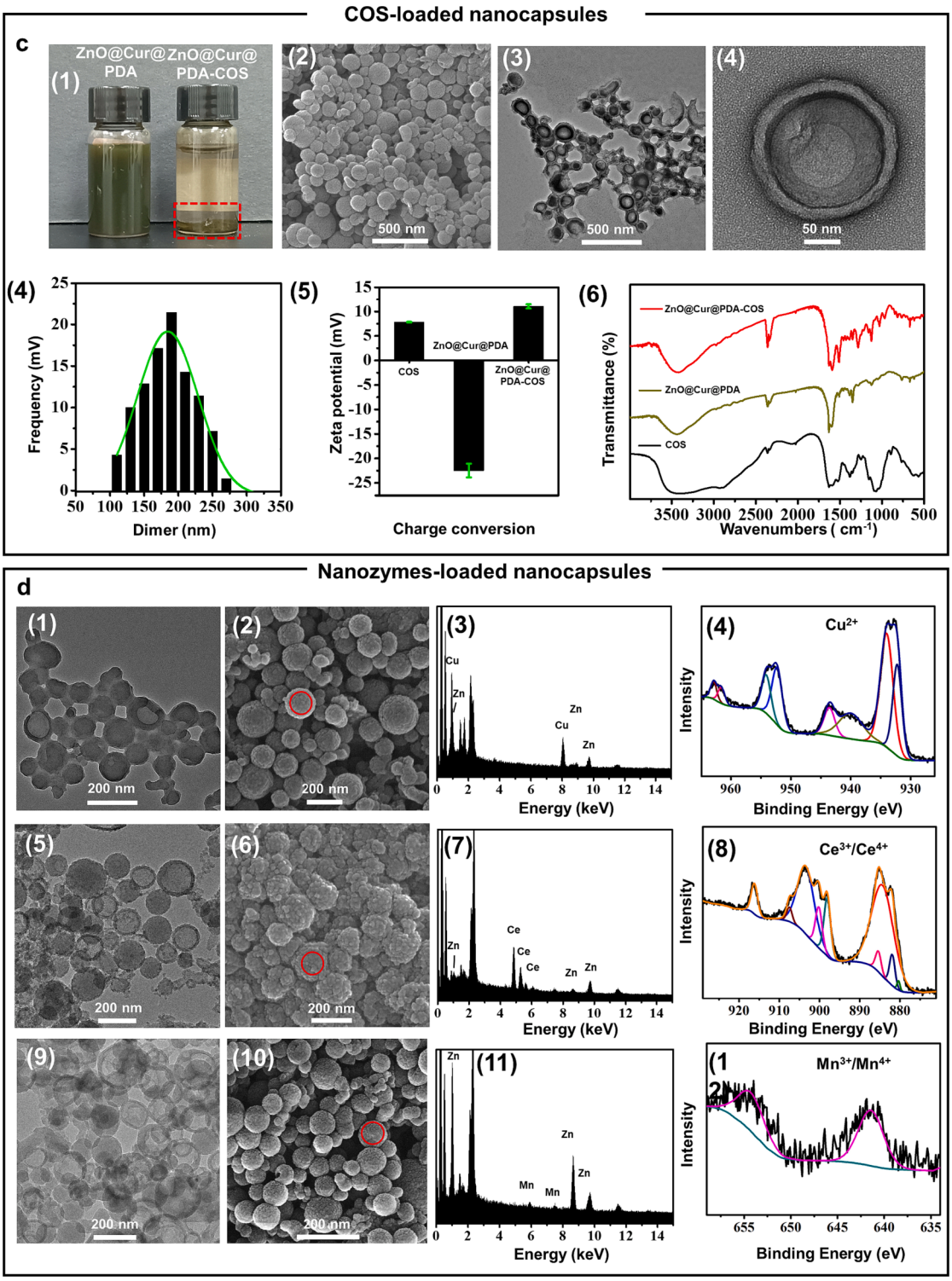

Fig. 7. **(a)** ZnO@Cur@PDA nanocapsules were used as templates to construct complex functional nanoparticles or pesticide delivery systems. **(b)** Ag–ZnO@Cur: Scheme and the topography characteristics of the curcumin assembled in the nanosilver dispersion solution (1); Scheme and the topography characteristics of the mixed solution containing curcumin and nanosilver assembled in the ZnO NP dispersion solution (2). **(c)** The colloid characteristics (1), morphology (2–4), particle size distribution (5), potential conversion (6) and infrared spectrum characteristics (7) of ZnO@Cur@PDA–COS. **(d)** Morphology (1, 2), element analysis in the microarea by EDS (3) and high–resolution Cu 2p XPS spectra (4) of Cu–ZnO@Cur@PDA; morphology (5, 6), element analysis in the microarea by EDS (7) and high–resolution Ce 2p XPS spectra (8) of Ce–ZnO@Cur@PDA; morphology (9, 10), element analysis in the microarea by EDS (11) and high–resolution Ce 2p XPS spectra (12) of Mn–ZnO@Cur@PDA.

by ZnO NPs. The ZnO@Cur-Beb NPs showed core–shell structure with an average particle size of 81.0 nm (Fig. S75). The loading efficiency of berberine hydrochloride of ZnO@Cur-Beb(mCur/mBeb = 1:1) was 28.2%±2.45%. ZnO@Cur-Beb NPs can selectively release berberine hydrochloride in PBS solution at different pH values (Fig. S76–S77). These nanoparticles with multiple active sites may be widely used in controlling plant disease or human disease by synergistic action.

4. Conclusion

In summary, we have established a new strategy for the assembly of nature small molecules (curcumin) mediated by inorganic nanoparticles (ZnO NPs) in water to form multifunctional nanocapsules with antibacterial activities against plant diseases. Our method has addressed the challenges in transforming unmodified small–molecule natural products such as curcumin into well–ordered nanostructures. The process is green and practical with low costs, meeting the environmental and economic expectations for pesticide applications. Detailed structural characterizations and physical property investigations of our nanocapsules were conducted. Both *in vitro* and *in vivo* bioactivity studies and their mechanistic implications were performed. In addition to direct use as potential nanopesticides, our multifunctional nanocapsules may also be further developed for the loading of other bioactive molecules to treat plant diseases. We expect our present work to open new avenues in turning natural small molecules into ordered structures for better performance as (nano)pesticides via environmentally benign and cost–effective processes.

Author Contributions

L.L., and S.Y. conceived the concept. L.L. designed the experiments and wrote the manuscript. L.L. carried out the preparation, characterization and performance test of nanoparticles, the interaction test between nanoparticles and bacteria or rice plants. Z.D., G.R., X.P., G.W. carried out the antibacterial activity test *in vitro* and *in vivo*. L.L. and G.R. carried out the safety experiment of nanoparticles on rice plants. Z.W., X.Z. helped data collection of the fluorescence imaging on bacteria. S.Y., Y.C. and Z.J. carried out lots of work in the framework, the logical relationship of the experiments results and conclusions, and the language of the manuscript. S.Y. and Y.C. supervised the research and revised the manuscript.

Declaration of Competing Interest

The authors declare that they have no known competing financial interests or personal relationships that could have appeared to influence the work reported in this paper.

Data availability

Data will be made available on request.

Acknowledgements

This work was financially supported by National Natural Science Foundation of China (32372610), National Key Research and Development Program of China (2022YFD1700300), the Guizhou Provincial S&T Project (2018[4007], ZK[2021]–General–144), and Program of Introducing Talents of Discipline to Universities of China (D20023, 111 Program).

Appendix A. Supplementary data

Supplementary data to this article can be found online at https://doi.org/10.1016/j.cej.2023.146041.

References

[1] D. Wang, N.B. Saleh, A. Byro, R. Zepp, E. Sahle-Demessie, T.P. Luxton, K.T. Ho, R. M. Burgess, M. Flury, J.C. White, C. Su, Nano-enabled pesticides for sustainable agriculture and global food security, Nat. Nanotechnol. 17 (4) (2022) 347–360, https://doi.org/10.1038/s41565-022-01082-8.
[2] P.L. Chariou, O.A. Ortega-Rivera, N.F. Steinmetz, Nanocarriers for the delivery of medical, veterinary, and agricultural active ingredients, ACS Nano 14 (3) (2020) 2678–2701, https://doi.org/10.1021/acsnano.0c00173.
[3] Y.H. Gao, Y. Liang, Z.Y. Zhou, J.L. Yang, Y.Y. Tian, J.F. Niu, G. Tang, J.Y. Tang, X. Chen, Y. Li, Y.S. Cao, Metal-organic framework nanohybrid carrier for precise pesticide delivery and pest management, Chem. Eng. J. 422 (2021) 9, https://doi.org/10.1016/j.cej.2021.130143.
[4] G. Tang, Y. Tian, Y. Gao, Z. Zhou, X. Chen, Y. Li, X. Yu, H. Wang, X. Li, Y. Cao, Supramolecular self-assembly of herbicides with reduced risks to the environment, ACS Nano 16 (3) (2022) 4892–4904, https://doi.org/10.1021/acsnano.2c00539.
[5] W. Liang, J. Cheng, J. Zhang, Q. Xiong, M. Jin, J. Zhao, pH-Responsive on-demand alkaloids release from core-shell zno@zif-8 nanosphere for synergistic control of bacterial wilt disease, ACS Nano 16 (2) (2022) 2762–2773, https://doi.org/10.1021/acsnano.1c09724.
[6] P.Y. Zhao, C.J. Wang, S.J. Zhang, L. Zheng, F.M. Li, C. Cao, L.D. Cao, Q.L. Huang, Fungicide-loaded mesoporous silica nanoparticles promote rice seedling growth by regulating amino acid metabolic pathways, J. Hazard. Mater. 425 (2022) 10, https://doi.org/10.1016/j.jhazmat.2021.127892.
[7] M.A. Farooq, F. Hannan, F. Islam, A. Ayyaz, N. Zhang, W. Chen, K. Zhang, Q. Huang, L. Xu, W. Zhou, The potential of nanomaterials for sustainable modern agriculture: present findings and future perspectives, Environ. Sci. Nano 9 (6) (2022) 1926–1951, https://doi.org/10.1039/D1EN01124C.
[8] A. Wang, J. Cui, Y. Wang, H. Zhu, N. Li, C. Wang, Y. Shen, P. Liu, B. Cui, C. Sun, X. Zhao, C. Wang, F. Gao, Z. Zeng, H. Cui, Preparation and characterization of a novel controlled-release nano-delivery system loaded with pyraclostrobin via high-pressure homogenization, Pest Manag. Sci. 76 (8) (2020) 2829–2837, https://doi.org/10.1002/ps.5833.
[9] Z. Pan, B. Cui, Z. Zeng, L. Feng, G. Liu, H. Cui, H. Pan, Lambda-Cyhalothrin Nanosuspension Prepared by the Melt Emulsification-High Pressure Homogenization Method, J. Nanomater. 2015 (2015) 123496. http://doi.org/10.1155/2015/123496.
[10] F. Corrias, A. Melis, A. Atzei, S. Marceddu, F. Dedola, A. Sirigu, R. Pireddu, F. Lai, A. Angioni, Zoxamide accumulation and retention evaluation after nanosuspension technology application in tomato plant, Pest Manag. Sci. 77 (7) (2021) 3508–3518, https://doi.org/10.1002/ps.6404.
[11] Z. Du, C. Wang, X. Tai, G. Wang, X. Liu, Optimization and characterization of biocompatible oil-in-water nanoemulsion for pesticide delivery, ACS Sustain. Chem. Eng. 4 (3) (2016) 983–991, https://doi.org/10.1021/acssuschemeng.5b01058.
[12] L. Wang, X. Li, G. Zhang, J. Dong, J. Eastoe, Oil-in-water nanoemulsions for pesticide formulations, J Colloid. Interf. Sci. 314 (1) (2007) 230–235, https://doi.org/10.1016/j.jcis.2007.04.079.
[13] C. Wang, B. Cui, L. Guo, A. Wang, X. Zhao, Y. Wang, C. Sun, Z. Zeng, Z. Heng, H. Chen, G. Liu, H. Cui, Fabrication and evaluation of lambda-cyhalothrin nanosuspension by one-step melt emulsification technique, Nanomaterials 9 (2019) 145, https://doi.org/10.3390/nano9020145.
[14] M. Usman, M. Farooq, A. Wakeel, A. Nawaz, S.A. Cheema, H.u. Rehman, I. Ashraf, M. Sanaullah, Nanotechnology in agriculture: current status, challenges and future opportunities, Sci. Total Environ. 721 (2020) 137778.
[15] E. Agathokleous, Z. Feng, I. Iavicoli, E.J. Calabrese, Nano-pesticides: a great challenge for biodiversity? The need for a broader perspective, Nano Today 30 (2020), 100808, https://doi.org/10.1016/j.nantod.2019.100808.
[16] Z. Xu, T. Tang, Q. Lin, J. Yu, C. Zhang, X. Zhao, M. Kah, L. Li, Environmental risks and the potential benefits of nanopesticides: a review, Environ. Chem. Lett. 20 (3) (2022) 2097–2108, https://doi.org/10.1007/s10311-021-01338-0.
[17] J.M. Buriak, L.M. Liz-Marzán, W.J. Parak, X. Chen, Nano and Plants, ACS Nano 16 (2) (2022) 1681–1684, https://doi.org/10.1021/acsnano.2c01131.
[18] M.B. Isman, Botanical insecticides, deterrents, and repellents in modern agriculture and an increasingly regulated world, Annu. Rev. Entomol. 51 (2006) 45–66, https://doi.org/10.1146/annurev.ento.51.110104.151146.
[19] M.B. Isman, Botanical Insecticides in the Twenty-First Century—Fulfilling Their Promise? Annu. Rev. Entomol. 65 (1) (2020) 233–249.
[20] P.G. Marrone, Pesticidal natural products - status and future potential, Pest Manag. Sci. 75 (9) (2019) 2325–2340, https://doi.org/10.1002/ps.5433.
[21] R. Pavela, F. Maggi, R. Iannarelli, G. Benelli, Plant extracts for developing mosquito larvicides: From laboratory to the field, with insights on the modes of action, Acta Trop. 193 (2019) 236–271, https://doi.org/10.1016/j.actatropica.2019.01.019.
[22] N. Umetsu, Y. Shirai, Development of novel pesticides in the 21st century, J. Pestic. Sci. 45 (1–2) (2020) 54–74, https://doi.org/10.1584/jpestics.D20-201.
[23] S.O. Duke, F.E. Dayan, The search for new herbicide mechanisms of action: Is there a 'holy grail'? Pest Manag. Sci. 78 (4) (2022) 1303–1313, https://doi.org/10.1002/ps.6726.
[24] X. Huang, M. Lv, H. Xu, Semisynthesis of novel N-acyl/sulfonyl derivatives of 5 (3,5)-(di)halogenocytisines/cytisine and their pesticidal activities against Mythimna separata Walker, Tetranychus cinnabarinus Boisduval, and Sitobion avenae Fabricius, Pest Manag. Sci. 75 (10) (2019) 2598–2609, https://doi.org/10.1002/ps.5375.

[25] B.A. Lorsbach, T.C. Sparks, R.M. Cicchillo, N.V. Garizi, D.R. Hahn, K.G. Meyer, Natural products: a strategic lead generation approach in crop protection discovery, Pest Manag. Sci. 75 (9) (2019) 2301–2309, https://doi.org/10.1002/ps.5350.

[26] F.A. Macias, F.J.R. Mejias, J.M.G. Molinillo, Recent advances in allelopathy for weed control: from knowledge to applications, Pest Manag. Sci. 75 (9) (2019) 2413–2436, https://doi.org/10.1002/ps.5355.

[27] M. Masi, E. Pannacci, E. Santoro, Z. Nadjia, S. Superchi, A. Evidente, Stoechanones A and B, Phytotoxic Copaane Sesquiterpenoids Isolated from Lavandula stoechas with Potential Herbicidal Activity against Amaranthus retroflexus, J. Nat. Prod. 83 (5) (2020) 1658–1665, https://doi.org/10.1021/acs.jnatprod.0c00182.

[28] K. Ujihara, The history of extensive structural modifications of pyrethroids, J. Pestic. Sci. 44 (3–4) (2019) 215–224, https://doi.org/10.1584/jpestics.D19-102.

[29] C. Zhou, X. Luo, N. Chen, L. Zhang, J. Gao, C-P Natural Products as Next-Generation Herbicides: Chemistry and Biology of Glufosinate, J. Agric. Food Chem. 68 (11) (2020) 3344–3353, https://doi.org/10.1021/acs.jafc.0c00052.

[30] M. Yuan, Z. Tian, X. Yin, X. Yuan, J. Gao, W. Yuan, A. Lu, Z. Wang, L. Li, Q. Wang, Structural Optimization of the Natural Product: Discovery of Almazoles C-D and Their Derivatives as Novel Antiviral and Anti-phytopathogenic Fungus Agents, J. Agric. Food Chem. 70 (50) (2022) 15693–15702, https://doi.org/10.1021/acs.jafc.2c05898.

[31] J. Dong, S.-S. Huang, Y.-N. Hao, Z.-W. Wang, Y.-X. Liu, Y.-Q. Li, Q.-M. Wang, Marine-natural-products for biocides development: first discovery of meridianin alkaloids as antiviral and anti-phytopathogenic-fungus agents, Pest Manag. Sci. 76 (10) (2020) 3369–3376, https://doi.org/10.1002/ps.5690.

[32] W. Guo, H. Yan, X. Ren, R. Tang, Y. Sun, Y. Wang, J. Feng, Berberine induces resistance against tobacco mosaic virus in tobacco, Pest Manag. Sci. 76 (5) (2020) 1804–1813, https://doi.org/10.1002/ps.5709.

[33] X. Hua, W. Liu, Y. Chen, J. Ru, S. Guo, X. Yu, Y. Cui, X. Liu, Y. Gu, C. Xue, Y. Liu, J. Sui, G. Wang, Synthesis, Fungicidal Activity, and Mechanism of Action of Pyrazole Amide and Ester Derivatives Based on Natural Products L-Serine and Waltherione Alkaloids, J. Agric. Food Chem. 69 (38) (2021) 11470–11484, https://doi.org/10.1021/acs.jafc.1c01346.

[34] S. Mao, C. Wu, Y. Gao, J. Hao, X. He, P. Tao, J. Li, S. Shang, Z. Song, J. Song, Pine Rosin as a Valuable Natural Resource in the Synthesis of Fungicide Candidates for Controlling Fusarium oxysporum on Cucumber, J. Agric. Food Chem. 69 (23) (2021) 6475–6484, https://doi.org/10.1021/acs.jafc.1c01887.

[35] G.-Z. Yang, J.-K. Zhu, X.-D. Yin, Y.-F. Yan, Y.-L. Wang, X.-F. Shang, Y.-Q. Liu, Z.-M. Zhao, J.-W. Peng, H. Liu, Design, Synthesis, and Antifungal Evaluation of Novel Quinoline Derivatives Inspired from Natural Quinine Alkaloids, J. Agric. Food Chem. 67 (41) (2019) 11340–11353, https://doi.org/10.1021/acs.jafc.9b04224.

[36] J. Zheng, R. Fan, H. Wu, H. Yao, Y. Yan, J. Liu, L. Ran, Z. Sun, L. Yi, L. Dang, P. Gan, P. Zheng, T. Yang, Y. Zhang, T. Tang, Y. Wang, Directed self-assembly of herbal small molecules into sustained release hydrogels for treating neural inflammation, Nat. Commun. 10 (1) (2019) 1604, https://doi.org/10.1038/s41467-019-09601-3.

[37] K. Zhi, J. Wang, H. Zhao, X. Yang, Self-assembled small molecule natural product gel for drug delivery: a breakthrough in new application of small molecule natural products, Acta Pharm. Sin. B 10 (5) (2020) 913–927, https://doi.org/10.1016/j.apsb.2019.09.009.

[38] Z. Wang, J. Lu, Z. Yuan, W. Pi, X. Huang, X. Lin, Y. Zhang, H. Lei, P. Wang, Natural Carrier-Free Binary Small Molecule Self-Assembled Hydrogel Synergize Antibacterial Effects and Promote Wound Healing by Inhibiting Virulence Factors and Alleviating the Inflammatory Response, Small 19 (5) (2023), https://doi.org/10.1002/smll.202205528.

[39] Y. Tian, G. Tang, Y. Gao, X.i. Chen, Z. Zhou, Y. Li, X. Li, H. Wang, X. Yu, L. Luo, Y. Cao, Carrier-Free Small Molecular Self-Assembly Based on Berberine and Curcumin Incorporated in Submicron Particles for Improving Antimicrobial Activity, ACS Appl. Mater. Interfaces 14 (8) (2022) 10055–10067.

[40] Y. Hou, L. Zou, Q. Li, M. Chen, H. Ruan, Z. Sun, X. Xu, J. Yang, G. Ma, Supramolecular assemblies based on natural small molecules: Union would be effective, Materials Today Bio. 15 (2022), 100327, https://doi.org/10.1016/j.mtbio.2022.100327.

[41] Bhawana, R.K. Basniwal, H.S. Buttar, V.K. Jain, N. Jain, Curcumin Nanoparticles: Preparation, Characterization, and Antimicrobial Study, J. Agric. Food Chem. 59 (5) (2011) 2056–2061.

[42] N.K. Bhatia, S. Kishor, N. Katyal, P. Gogoi, P. Narang, S. Deep, Effect of pH and temperature on conformational equilibria and aggregation behaviour of curcumin in aqueous binary mixtures of ethanol, RSC Adv. 6 (105) (2016) 103275–103288, https://doi.org/10.1039/C6RA24256A.

[43] A.K. Sahu, J. Mishra, A.K. Mishra, Introducing Tween-curcumin niosomes: preparation, characterization and microenvironment study, Soft Matter 16 (7) (2020) 1779–1791.

[44] K. Nagahama, T. Kumano, N. Oyama, J. Kawakami, Curcumisome nanovesicles generated by self-assembly of curcumin amphiphiles toward cancer theranostics, Biomater. SCI-UK 3 (12) (2015) 1566–1578, https://doi.org/10.1039/C5BM00212E.

[45] Y. Li, Q. Zou, C. Yuan, S. Li, R. Xing, X. Yan, Amino Acid Coordination Driven Self-Assembly for Enhancing both the Biological Stability and Tumor Accumulation of Curcumin, Angew. Chem. Int. Ed. Engl. 57 (52) (2018) 17084–17088, https://doi.org/10.1002/anie.201810087.

[46] S. Wong, J. Zhao, C. Cao, C.K. Wong, R.P. Kuchel, S. De Luca, J.M. Hook, C. J. Garvey, S. Smith, J. Ho, M.H. Stenzel, Just add sugar for carbohydrate induced self-assembly of curcumin, Nat. Commun. 10 (1) (2019) 582, https://doi.org/10.1038/s41467-019-08402-y.

[47] W. Park, H. Shin, B. Choi, W.-K. Rhim, K. Na, D. Keun Han, Advanced hybrid nanomaterials for biomedical applications, Prog. Mater Sci. 114 (2020), 100686, https://doi.org/10.1016/j.pmatsci.2020.100686.

[48] W. Al Zoubi, M.P. Kamil, S. Fatimah, N. Nashrah, Y.G. Ko, Recent advances in hybrid organic-inorganic materials with spatial architecture for state-of-the-art applications, Prog. Mater Sci. 112 (2020), 100663, https://doi.org/10.1016/j.pmatsci.2020.100663.

[49] H. Zheng, Y. Li, H. Liu, X. Yin, Y. Li, Construction of heterostructure materials toward functionality, Chem. Soc. Rev. 40 (9) (2011) 4506–4524, https://doi.org/10.1039/C0CS00222D.

[50] M. Heinlaan, A. Ivask, I. Blinova, H.-C. Dubourguier, A. Kahru, Toxicity of nanosized and bulk ZnO, CuO and TiO2 to bacteria Vibrio fischeri and crustaceans Daphnia magna and Thamnocephalus platyurus, Chemosphere 71 (7) (2008) 1308–1316.

[51] C.O. Dimkpa, J.E. McLean, D.E. Latta, E. Manangon, D.W. Britt, W.P. Johnson, M. I. Boyanov, A.J. Anderson, CuO and ZnO nanoparticles: phytotoxicity, metal speciation, and induction of oxidative stress in sand-grown wheat, J. Nanopart. Res. 14 (9) (2012), https://doi.org/10.1007/s11051-012-1125-9.

[52] C.W. Lee, S. Mahendra, K. Zodrow, D. Li, Y.-C. Tsai, J. Braam, P.J.J. Alvarez, DEVELOPMENTAL PHYTOTOXICITY OF METAL OXIDE NANOPARTICLES TO ARABIDOPSIS THALIANA, Environmental Toxicology and Chemistry 29(3) (2010) 669-675.http://doi.org/10.1002/etc.58.

[53] J. Zhou, Z. Lin, M. Penna, S. Pan, Y. Ju, S. Li, Y. Han, J. Chen, G. Lin, J. J. Richardson, I. Yarovsky, F. Caruso, Particle engineering enabled by polyphenol-mediated supramolecular networks, Nat. Commun. 11 (1) (2020) 4804, https://doi.org/10.1038/s41467-020-18589-0.

[54] J. Chen, Y. Luo, C. Wei, S. Wu, R. Wu, S. Wang, D. Hu, B. Song, Novel sulfone derivatives containing a 1,3,4-oxadiazole moiety: design and synthesis based on the 3D-QSAR model as potential antibacterial agent, Pest Manag. Sci. 76 (9) (2020) 3188–3198, https://doi.org/10.1002/ps.5873.

[55] Q. Zhang, Y.-X. Deng, H.-X. Luo, C.-Y. Shi, G.M. Geise, B.L. Feringa, H. Tian, D.-H. Qu, Assembling a Natural Small Molecule into a Supramolecular Network with High Structural Order and Dynamic Functions, J. Am. Chem. Soc. 141 (32) (2019) 12804–12814, https://doi.org/10.1021/jacs.9b05740.

[56] Z. Zhang, C. Liu, H. Zhang, Z.-K. Xu, F. Ju, C. Yu, Y. Xu, Ultrafast Interfacial Self-Assembly toward Supramolecular Metal-Organic Films for Water Desalination, Adv. Sci. 9 (24) (2022) 2201624, https://doi.org/10.1002/advs.202201624.

[57] G. Angelini, A. Pasc, C. Gasbarri, Curcumin in silver nanoparticles aqueous solution: Kinetics of keto-enol tautomerism and effects on AgNPs, Colloid Surface A 603 (2020) 125235.

[58] J.R. Bathi, F. Moazeni, V.K.K. Upadhyayula, I. Chowdhury, S. Palchoudhury, G. E. Potts, V. Gadhamshetty, Behavior of engineered nanoparticles in aquatic environmental samples: Current status and challenges, Sci. Total Environ. 793 (2021), 148560, https://doi.org/10.1016/j.scitotenv.2021.148560.

[59] Y. Zhang, Y. Chen, P. Westerhoff, J. Crittenden, Impact of natural organic matter and divalent cations on the stability of aqueous nanoparticles, Water Res. 43 (17) (2009) 4249–4257, https://doi.org/10.1016/j.watres.2009.06.005.

[60] U. Stoeck, S. Krause, V. Bon, I. Senkovska, S. Kaskel, A highly porous metal–organic framework, constructed from a cuboctahedral super-molecular building block, with exceptionally high methane uptake, Chem. Commun. 48 (88) (2012) 10841.

[61] Prateeksha, C.V. Rao, A.K. Das, S.K. Barik, B.N. Singh, Singh, ZnO/Curcumin Nanocomposites for Enhanced Inhibition of Pseudomonas aeruginosa Virulence via LasR-RhlR Quorum Sensing Systems, Mol. Pharm. 16 (8) (2019) 3399–3413.

[62] N. Portolés-Gil, A. Lanza, N. Aliaga-Alcalde, J.A. Ayllón, M. Gemmi, E. Mugnaioli, A.M. López-Periago, C. Domingo, Crystalline Curcumin bioMOF Obtained by Precipitation in Supercritical CO2 and Structural Determination by Electron Diffraction Tomography, ACS Sustain. Chem. Eng. 6 (9) (2018) 12309–12319, https://doi.org/10.1021/acssuschemeng.8b02738.

[63] G. Moradi, S. Zinadini, L. Rajabi, A. Ashraf Derakhshan, Removal of heavy metal ions using a new high performance nanofiltration membrane modified with curcumin boehmite nanoparticles, Chem. Eng. J. 390 (2020), 124546, https://doi.org/10.1016/j.cej.2020.124546.

[64] B. Mandal, A.P. Rameshbabu, S.R. Soni, A. Ghosh, S. Dhara, S. Pal, In Situ Silver Nanowire Deposited Cross-Linked Carboxymethyl Cellulose: A Potential Transdermal Anticancer Drug Carrier, ACS Appl. Mater. Interfaces 9 (42) (2017) 36583–36595.

[65] J. Mu, C. Shao, Z. Guo, Z. Zhang, M. Zhang, P. Zhang, B. Chen, Y. Liu, High Photocatalytic Activity of ZnO−Carbon Nanofiber Heteroarchitectures, ACS Appl. Mater. Interfaces 3 (2) (2011) 590–596, https://doi.org/10.1021/am101171a.

[66] J. Yu, X. Yu, Hydrothermal Synthesis and Photocatalytic Activity of Zinc Oxide Hollow Spheres, Environ. Sci. Tech. 42 (13) (2008) 4902–4907, https://doi.org/10.1021/es800036n.

[67] T.M. Kolev, E.A. Velcheva, B.A. Stamboliyska, M. Spiteller, DFT and experimental studies of the structure and vibrational spectra of curcumin, Int. J. Quantum Chem 102 (6) (2005) 1069–1079, https://doi.org/10.1002/qua.20469.

[68] X.-Z. Zhao, T. Jiang, L. Wang, H. Yang, S. Zhang, P. Zhou, Interaction of curcumin with Zn(II) and Cu(II) ions based on experiment and theoretical calculation, J. Mol. Struct. 984 (1-3) (2010) 316–325.

[69] Z.H. Xing, J.H. Wei, T.Y. Cheang, Z.R. Wang, X. Zhou, S.S. Wang, W. Chen, S. M. Wang, J.H. Luo, A.W. Xu, Bifunctional pH-sensitive Zn(ii)-curcumin nanoparticles/siRNA effectively inhibit growth of human bladder cancer cells in vitro and in vivo, J. Mater. Chem. B 2 (18) (2014) 2714–2724, https://doi.org/10.1039/c3tb21625j.

[70] B. Zebib, Z. Mouloungui, V. Noirot, Stabilization of curcumin by complexation with divalent cations in glycerol/water system, Bioinorg. Chem. Appl. 2010 (2010) 1–8.
[71] M.K. Hazra, S. Roy, B. Bagchi, Hydrophobic hydration driven self-assembly of curcumin in water: similarities to nucleation and growth under large metastability, and an analysis of water dynamics at heterogeneous surfaces, J. Chem. Phys. 141 (18) (2014).
[72] J.H. Jordan, B.C. Gibb, Molecular containers assembled through the hydrophobic effect, Chem. Soc. Rev. 44 (2) (2015) 547–585, https://doi.org/10.1039/c4cs00191e.
[73] B. Guo, E. Middha, B. Liu, Solvent Magic for Organic Particles, ACS Nano 13 (3) (2019) 2675–2680.
[74] L.E. Franken, Y. Wei, J. Chen, E.J. Boekema, D. Zhao, M.C.A. Stuart, B.L. Feringa, Solvent Mixing To Induce Molecular Motor Aggregation into Bowl-Shaped Particles: Underlying Mechanism, Particle Nature, and Application To Control Motor Behavior, J. Am. Chem. Soc. 140 (25) (2018) 7860–7868, https://doi.org/10.1021/jacs.8b03045.
[75] W.-D. Jang, D. Yim, I.-H. Hwang, Photofunctional hollow nanocapsules for biomedical applications, J. Mater. Chem. B 2 (16) (2014) 2202–2211, https://doi.org/10.1039/c4tb00076e.
[76] S. Li, Y. Ju, J. Zhou, K.F. Noi, A.J. Mitchell, T. Zheng, S.J. Kent, C.J.H. Porter, F. Caruso, Quantitatively Tracking Bio-Nano Interactions of Metal-Phenolic Nanocapsules by Mass Cytometry, ACS Appl. Mater. Interfaces 13 (30) (2021) 35494–35505, https://doi.org/10.1021/acsami.1c09406.
[77] Y. Liu, J. Yang, Z. Zhao, J. Li, R. Zhang, F. Yao, Formation and characterization of natural polysaccharide hollow nanocapsules via template layer-by-layer self-assembly, J Colloid. Interf. Sci. 379 (2012) 130–140, https://doi.org/10.1016/j.jcis.2012.04.058.
[78] R.J. Wilson, Y. Hui, A.K. Whittaker, C.-X. Zhao, Facile bioinspired synthesis of iron oxide encapsulating silica nanocapsules, J Colloid. Interf. Sci. 601 (2021) 78–84, https://doi.org/10.1016/j.jcis.2021.05.021.
[79] X. Yan, L. Chai, E. Fleury, F. Ganachaud, J. Bernard, 'Sweet as a Nut': Production and use of nanocapsules made of glycopolymer or polysaccharide shell, Prog. Polym. Sci. 120 (2021) 101429.
[80] Y. Dong, Y. Yang, C. Lin, D. Liu, Frame-Guided Assembly of Amphiphiles, Acc. Chem. Res. 55 (14) (2022) 1938–1948, https://doi.org/10.1021/acs.accounts.2c00234.
[81] L. Li, R. Sun, R. Zheng, Tunable morphology and functionality of multicomponent self-assembly: A review, Mater. Design 197 (2021), 109209, https://doi.org/10.1016/j.matdes.2020.109209.
[82] W. Foster, K. Miyazawa, T. Fukuma, H. Kusumaatmaja, K. Voïtchovsky, Self-assembly of small molecules at hydrophobic interfaces using group effect, Nanoscale 12 (9) (2020) 5452–5463, https://doi.org/10.1039/C9NR09505E.
[83] S. Auychaipornlert, P. Prayurnprohm Lawanprasert, S. Piriyaprasarth, P. Sithisarn, Interfacial tension of turmeric nanoparticles, ScienceAsia 44(1) (2018) 11–17, https://doi.org/10.2306/scienceasia1513-1874.2018.44.011.
[84] P. Chandrangsu, C. Rensing, J.D. Helmann, Metal homeostasis and resistance in bacteria, Nat. Rev. Microbiol. 15 (6) (2017) 338–350, https://doi.org/10.1038/nrmicro.2017.15.
[85] G.W. Sundin, N. Wang, Antibiotic Resistance in Plant-Pathogenic Bacteria, Annu. Rev. Phytopathol. 56 (1) (2018) 161–180, https://doi.org/10.1146/annurev-phyto-080417-045946.
[86] J.F. Xiong, P.Y. Xu, Z.S. Wang, D.G. Pang, Study on the subchronic oral toxicity of bismerthiazol on rats, Mod. Prev. Med. 1 (2008) 127–129, https://doi.org/10.1016/j.fct.2012.11.003.
[87] X. Liang, Y. Duan, X. Yu, J. Wang, M. Zhou, Photochemical degradation of bismerthiazol: structural characterisation of the photoproducts and their inhibitory activities against Xanthomonas oryzae pv. oryzae: photochemicaldegradationofbismerthiazoland inhibitoryactivities against Xoo, Pest Manag. Sci. 72 (5) (2016) 997–1003.
[88] Y. Honglian, L. Huanliang, Z. Wei, S. Xiaojun, G. Xiujie, M.a. Kefeng, W. Kun, C. Bo, F. Yanjun, X.i. Zhuge, Thyroid-disrupting effects and mechanism of thiazole-Zn-induced thyroid cell hypertrophy and hyperplasia in male Sprague-Dawley rats, Ecotoxicol. Environ. Saf. 196 (2020) 110544.
[89] M. Jain, A. Marfatia, N. Imam, D. Ray, V.K. Aswal, N.Y. Patel, V.H. Raval, S. K. Kailasa, N.I. Malek, Ionic liquid-based catanionic vesicles: a de novo system to judiciously improve the solubility, stability and antimicrobial activity of curcumin, J. Mol. Liq. 341 (2021), 117396, https://doi.org/10.1016/j.molliq.2021.117396.
[90] J. Shan, X. Li, K. Yang, W. Xiu, Q. Wen, Y. Zhang, L. Yuwen, L. Weng, Z. Teng, L. Wang, Efficient bacteria killing by cu2ws4 nanocrystals with enzyme-like properties and bacteria-binding ability, ACS Nano 13 (12) (2019) 13797–13808, https://doi.org/10.1021/acsnano.9b03868.
[91] P. Delparastan, K.G. Malollari, H. Lee, P.B. Messersmith, Direct evidence for the polymeric nature of polydopamine, Angew. Chem. Int. Ed. 58 (4) (2019) 1077–1082.
[92] H. Choi, S.H. Cho, S.K. Hahn, Urease-powered polydopamine nanomotors for intravesical therapy of bladder diseases, ACS Nano 14 (6) (2020) 6683–6692, https://doi.org/10.1021/acsnano.9b09726.
[93] S. Xu, X. Pan, J. Luo, J. Wu, Z. Zhou, X. Liang, Y. He, M. Zhou, Effects of phenazine-1-carboxylic acid on the biology of the plant-pathogenic bacterium Xanthomonas oryzae pv. oryzae, Pestic. Biochem. Physiol. 117 (2015) 39–46, https://doi.org/10.1016/j.pestbp.2014.10.006.
[94] S. Xu, X. Zhao, F. Liu, Y. Cao, B.i. Wang, X. Wang, M. Yin, Q. Wang, X.u. Feng, Crucial role of oxidative stress in bactericidal effect of parthenolide against Xanthomonas oryzae pv. oryzae: role of oxidative stress in bactericidal effect of parthenolide, Pest Manag. Sci. 74 (12) (2018) 2716–2723.
[95] H. Hatcher, R. Planalp, J. Cho, F.M. Torti, S.V. Torti, Curcumin: From ancient medicine to current clinical trials, Cell. Mol. Life Sci. 65 (11) (2008) 1631–1652.
[96] A. Sirelkhatim, S. Mahmud, A. Seeni, N.H.M. Kaus, L.C. Ann, S.K.M. Bakhori, H. Hasan, D. Mohamad, Review on zinc oxide nanoparticles: antibacterial activity and toxicity mechanism, Nano-Micro Lett. 7 (3) (2015) 219–242.
[97] Y. Liu, K. Ai, L. Lu, Polydopamine and its derivative materials: synthesis and promising applications in energy, environmental, and biomedical fields, Chem. Rev. 114 (9) (2014) 5057–5115.
[98] Z. Deng, B. Shang, B. Peng, Polydopamine based colloidal materials: synthesis and applications, Chem. Rec. 18 (4) (2018) 410–432, https://doi.org/10.1002/tcr.201700051.
[99] Y.-J. Wang, M.-H. Pan, A.-L. Cheng, L.-I. Lin, Y.-S. Ho, C.-Y. Hsieh, J.-K. Lin, Stability of curcumin in buffer solutions and characterization of its degradation products, J. Pharm. Biomed. Anal. 15 (12) (1997) 1867–1876.
[100] J.-H. Lin, C.-J. Yu, Y.-C. Yang, W.-L. Tseng, Formation of fluorescent polydopamine dots from hydroxyl radical-induced degradation of polydopamine nanoparticles, PCCP 17 (23) (2015) 15124–15130.
[101] K. Wakamatsu, Y. Nakanishi, N. Miyazaki, L. Kolbe, S. Ito, UVA-induced oxidative degradation of melanins: fission of indole moiety in eumelanin and conversion to benzothiazole moiety in pheomelanin, Pigment Cell Melanoma Res. 25 (4) (2012) 434–445, https://doi.org/10.1111/j.1755-148X.2012.01011.x.
[102] C. Hu, F. Zhang, Q. Kong, Y. Lu, B. Zhang, C. Wu, R. Luo, Y. Wang, Synergistic chemical and photodynamic antimicrobial therapy for enhanced wound healing mediated by multifunctional light-responsive nanoparticles, Biomacromolecules 20 (12) (2019) 4581–4592, https://doi.org/10.1021/acs.biomac.9b01401.
[103] J.Q. Xi, G. Wei, L.F. An, Z.B. Xu, Z.L. Xu, L. Fan, L.Z. Gao, Copper/carbon hybrid nanozyme: tuning catalytic activity by the copper state for antibacterial therapy, Nano Lett. 19 (11) (2019) 7645–7654, https://doi.org/10.1021/acs.nanolett.9b02242.